View Article Online
View Journal

Dalton Transactions

An international journal of inorganic chemistry

Accepted Manuscript

This article can be cited before page numbers have been issued, to do this please use: A. Karabut, H. Zhydachevska, L. Wachnicki, V. Hreb, L. Vasylechko, Y. Hizhnyi, T. Shevtsova, A. Luchechko, A. Pieniek, M. Berkowski and Y. Zhydachevskyy, *Dalton Trans.*, 2026, DOI: 10.1039/D6DT00337K.

ROYAL SOCIETY OF CHEMISTRY

rsc.li/dalton

Tuning the crystal structure, optical band gap and persistent luminescence performance of Cr^{3+}-doped $LiGa_5O_8$ spinel by adding aluminium and indium

View Article Online
DOI: 10.1039/D6DT00337K

Anastasiia Karabut[a], Halyna Zhydachevska[a], Łukasz Wachnicki[a], Vasyl Hreb[b], Leonid Vasylechko[b,*], Yuriy Hizhnyi[c,d], Tetiana Shevtsova[c], Andriy Luchechko[e], Agnieszka Pieniążek[a], Marek Berkowski[a], Yaroslav Zhydachevskyy[a,f,*]

[a] Institute of Physics, Polish Academy of Sciences, aleja Lotników 32/46, Warsaw 02-668, Poland
Email: zhydach@ifpan.edu.pl

[b] Lviv Polytechnic National University, S. Bandera Str. 12, Lviv 79013, Ukraine
Email: leonid.o.vasylechko@lpnu.ua

[c] Donetsk Institute for Physics and Engineering of NAS of Ukraine, Kyiv 03028, Ukraine

[d] Taras Shevchenko National University of Kyiv, Volodymyrska Str. 64/13 Kyiv 01601, Ukraine

[e] Ivan Franko National University of Lviv, Tarnavskogo Str. 107, Lviv 79017, Ukraine

[f] Berdyansk State Pedagogical University, Shmidta Str. 4, Berdyansk 71100, Ukraine

* Corresponding authors

Abstract

The possibility of tuning the optical band gap, crystal structure and persistent luminescence performance of Cr^{3+}-doped $LiGa_5O_8$ spinel by partially replacing Ga with Al and/or In has been studied extensively. For this purpose, a series of Cr^{3+}-doped $Li(Ga_{1-x-y}Al_xIn_y)_5O_8$ ($x = 0…0.5$; $y = 0…0.1$) microcrystalline phosphors were synthesised using a conventional solid-state reaction method and characterised by powder X-ray diffraction, SEM-EDX and luminescence techniques. The DFT-based electronic structure calculations were carried out for the same $Li(Ga_{1-x-y}Al_xIn_y)_5O_8$ compositions, and the results were compared with the experimental ones. Based on the studies performed, the mechanism of Al and In incorporation into the $LiGa_5O_8$ spinel structure, as well as the tuning of the crystal lattice parameters, local structure of M^{3+} (M = Ga, Al, In) cations and optical band gap of the material have been established. The multicentre structure and the broadening of the local structural disorder of the octahedrally coordinated Cr^{3+} centres observed in this case have been confirmed by the high-resolution, low-temperature photoluminescence measurements. Band gap engineering through alterations in the chemical composition of the $LiGa_5O_8$ spinel, as well as the depth of the native point defects

responsible for charge trapping, allows for the efficient tuning of the thermoluminescent and persistent luminescent properties of $Li(Ga_{1-x-y}Al_xIn_y)_5O_8:Cr^{3+}$ phosphors. Thus, the room-temperature persistent luminescence performance of the phosphors modified by the addition of Al and annealing in an oxygen-free atmosphere was increased threefold compared to the pristine $LiGa_5O_8:Cr^{3+}$ phosphor synthesised under the same conditions.

1. Introduction

Lithium-gallium spinel ($LiGa_5O_8$) activated with rare-earth (RE) or transition metal (TM) ions is a known crystalline phosphor having long-lasting persistent luminescence (PersL) or mechanoluminescence (ML) properties.[1-3] In particular, when activated with Cr^{3+}, it exhibits persistent luminescence in the deep red spectral region at about 700 nm.[4-6] The radiation storage properties allowing the persistent luminescence or mechanoluminescence of the material are caused by intrinsic point defects, such as cation antisites, cation and oxygen vacancies that are highly probable in this spinel compound.[7-9] These defects reveal themselves through the thermally stimulated luminescence (TSL) that occurs in the material after exposure to UV or higher energy light.

It is well known that the band gap engineering of a crystalline host lattice allows to tune the TSL and PersL properties of phosphors over a wide range (see *e.g.* Zhydachevskyy et al.).[10] Such a possibility has recently been demonstrated for Ga-containing oxides, such as γ-$Ga_2O_3:Cr$, by alloying with indium or aluminium oxides.[11] In addition to engineering of the band gap, replacing one host cation with another can also produce disorder in the local structure, thereby broadening the spectral properties of activator ions or intrinsic point defects in the host lattice.[12]

As regards the possibility of tuning the $LiGa_5O_8$ host, not much is known. It is known, however, that the aluminium-based counterpart, $LiAl_5O_8$, has the same type of structure, and a continuous series of $Li(Ga_{1-x}Al_x)_5O_8$ solid solutions exists, which allows for a gradual change in the crystal structure parameters of these spinel compounds.[13, 14] At the same time, there is nothing known on the possibility of introducing indium onto either the $LiGa_5O_8$ or $LiAl_5O_8$ compounds to tune the band gap and trap depth in this host. It is also unclear whether the $LiGa_5O_8$ host is optimal for long-lasting PersL and whether it can be improved by modifying the host with aluminium or indium. Therefore, the present work explores the potential of engineering the band gap and local structure to adjust the thermoluminescence and persistent luminescence properties of $Li(Ga,Al,In)_5O_8:Cr^{3+}$ phosphors. For this purpose, a series of $Li(Ga_{1-x-y}Al_xIn_y)_5O_8:Cr^{3+}$ compounds with various compositions (x values ranging from 0 to 0.5 and y values ranging from 0 to 0.1) were synthesised and thoroughly characterised using the

powder XRD, SEM-EDX and luminescence techniques. The DFT-based electronic structure calculations of $Li(Ga_{1-x-y}Al_xIn_y)_5O_8$ alloys with x and y values being the same as in synthesised samples were carried out to strengthen the inferences obtained from experimental studies.

The electronic structure of pure $LiGa_5O_8$ spinel was already studied previously by first-principles methods,[15-17] while the electronic properties of native defects in $LiGa_5O_8$ were studied computationally.[8, 7] However, to the best of our knowledge, no results on the electronic structure of $Li(Ga_{1-x-y}Al_xIn_y)_5O_8$ alloys have been published so far.

2. Experimental Methods

Samples, experimental and computational techniques. The studied Cr^{3+}-doped $LiGa_5O_8$-based microcrystalline samples were synthesised by a conventional solid-state reaction technique starting from high-purity Li_2CO_3 (99.99%), Ga_2O_3 (99.99%), Al_2O_3 (99.999%), In_2O_3 (99.999%) and Cr_2O_3 (99.999%) microcrystalline powders. The starting powders were weighed in the appropriate proportions corresponding to the lithium-rich composition of $Li_{1.02}Ga_5O_8$ and thoroughly ground in an agate mortar. The 2% excess of Li_2CO_3 was proven experimentally to be the optimal composition for obtaining the single-phase spinel under the given synthesis conditions. Specifically, when the stoichiometric ratio of Li_2CO_3 and Ga_2O_3 was used, alongside the main $LiGa_5O_8$ spinel, residual traces of γ-Ga_2O_3 were revealed in the final products. The Cr_2O_3 dopant at a concentration 0.5 mol.% was added at the expense of Li_2CO_3 (which was already in excess). The same mixture of 99.5% Li_2CO_3 + 0.5% Cr_2O_3 prepared in a larger amount was used for preparing all the Cr-doped samples to ensure the same chromium concentration in the samples (see Table 1). The final mixtures were pre-synthesised at 800 °C for 2 hours, then thoroughly ground once more in an agate mortar and finally synthesised at 1300 °C for 3 hours. Both the preliminary and final syntheses were performed in alundum crucibles under normal air conditions.

Additionally, in order to study the effect of reducing annealing, the samples were annealed in a high vacuum at 1000 °C for 2 hours. For this, a part of each powder sample was annealed in alundum crucibles in a closed quartz reactor that was continuously pumped out up to a pressure of 10^{-5} mbar.

X-ray powder diffraction (XRD) characterization of the synthesised materials was performed by an Aeris benchtop powder diffractometer (Malvern Panalytical) equipped with a PIXcel^{1D} strip detector. Experimental diffraction data were collected using filtered Cu K_α radiation (λ = 1.54185 Å) in a 2θ range of 6–105 degrees with a 2θ step of 0.02°. Lattice parameters, coordinates and displacement parameters of atoms were derived from experimental XRD patterns by full profile Rietveld refinement using the WinCSD software package.[18]

The scanning electron microscopy (SEM) and the energy-dispersive X-ray spectroscopy (EDX) analyses were carried out by a Hitachi SU-70 scanning electron microscope coupled with a Thermo Fisher Scientific Energy Dispersion X-ray spectrometer with a Li-drift silicon X-ray detector.

Table 1. List of the Cr^{3+}-doped $Li(Ga_{1-x-y}Al_xIn_y)_5O_8$ samples studied.

Sample notation	Composition			Phase composition
	Chemical formula	Al content (%)	In content (%)	
0% Al	$LiGa_5O_8$:Cr(0.5%)	0	0	Pure spinel
5% In	$Li(Ga_{0.95}In_{0.05})_5O_8$:Cr(0.5%)	0	5	Almost pure spinel
10% In	$Li(Ga_{0.9}In_{0.1})_5O_8$:Cr(0.5%)	0	10	Spinel + γ-$(Ga,In)O_3$
5% Al	$Li(Ga_{0.95}Al_{0.05})_5O_8$:Cr(0.5%)	5	0	Pure spinel
10% Al	$Li(Ga_{0.9}Al_{0.1})_5O_8$:Cr(0.5%)	10	0	Pure spinel
5% Al 5% In	$Li(Ga_{0.9}Al_{0.05}In_{0.05})_5O_8$:Cr(0.5%)	5	5	Pure spinel
7% Al 3% In	$Li(Ga_{0.9}Al_{0.07}In_{0.03})_5O_8$:Cr(0.5%)	7	3	Pure spinel
14% Al 6% In	$Li(Ga_{0.8}Al_{0.14}In_{0.06})_5O_8$:Cr(0.5%)	14	6	Spinel + γ-$(Ga,In)O_3$
20% Al	$Li(Ga_{0.8}Al_{0.2})_5O_8$:Cr(0.5%)	20	0	Pure spinel
30% Al	$Li(Ga_{0.7}Al_{0.3})_5O_8$:Cr(0.5%)	30	0	Pure spinel
40% Al	$Li(Ga_{0.6}Al_{0.4})_5O_8$:Cr(0.5%)	40	0	Pure spinel
50% Al	$Li(Ga_{0.5}Al_{0.5})_5O_8$:Cr(0.5%)	50	0	Pure spinel

The photoluminescence (PL) and the photoluminescence excitation (PLE) spectra were measured using a Horiba/Jobin-Yvon Fluorolog-3 spectrofluorometer with a 450 W continuous spectrum xenon lamp for excitation. The emission was detected by a Hamamatsu R928P photomultiplier operating in a photon counting mode. The PL spectra were corrected for the spectral response of the used system. The afterglow (PersL) decay kinetics and the thermally stimulated luminescence (TSL) curves were measured using the same Fluorolog-3 spectrofluorometer in the real-time decay mode. The TSL measurements in the temperature range of 77–700 K were done using a Linkam THMS600 temperature stage using linear heating at a rate of 1 K/s. The photoluminescence quantum efficiency measurements were performed using the same spectrofluorometer and a Horiba Quant-phi integrating sphere. The quantum

efficiency (QE) was calculated as the ratio of the number of emitted photons to that of the absorbed photons similarly as it is described in Zhydachevskyy et al.[19] The PLE measurements using synchrotron radiation were performed using the facilities of PETRA III P66 beamline of the Deutsches Elektronen-Synchrotron DESY, Hamburg, Germany.[20]

The DFT-based electronic structure calculations of $Li(Ga_{1-x-y}Al_xIn_y)_5O_8$ alloys were performed using the supercell approach. The supercells were constructed by 2×2×2 replication of the unit cell of $Li(Ga_{1-x-y}Al_xIn_y)_5O_8$ crystal, resulting in a structure containing 448 atoms (Fig. S4). All supercells were assigned the primitive symmetry group P1. The number of cationic substitutions modelled in the supercells for each x and y is listed in Table S1. For each x and y, 10 structures were generated with random distributions of In_{Ga} and Al_{Ga} substitutions. All structures were subjected to geometrical optimisation, and total energies were calculated for each configuration. The optical spectra were calculated only for the structures with the lowest total energy among all configurations modelled for each x and/or y value.

The electronic structure calculations were performed using the DFT-based band-periodic pseudopotential method implemented in the CASTEP program, which is part of the Materials Studio package.[21] Geometry optimisations accounted for exchange-correlation effects using the GGA-PBE approximation.[22] Atomic positions were optimised using the Broyden-Fletcher-Goldfarb-Shenno (BFGS) minimization algorithm[23] with the convergence criterion for energy and force on the atoms, which were set to 10^{-5} eV per atom and 0.03 eV/Å per atom, respectively. Geometry optimizations were performed only for the Γ point of the Brillouin zone.

To overcome the underestimation of the band gap energies E_g by the PBE functional, the optical (inter-band) absorption spectra were calculated using the GGA-PBE plus Hubbard U (GGA + U) approach.[24] The on-site Coulomb corrections (U) for specific orbitals (O 2p: 6.7 eV, Ga 3d: 7.0 eV, Al 3d: 7.0 eV, In 3d: 5.0 eV) were selected from the condition of the best agreement between the calculated and experimental band gaps for Ga_2O_3, Al_2O_3 and In_2O_3 crystals (see details in Vasylechko at al).[25]

For the calculations of the optical absorption spectra the Brillouin zone was sampled using a 2×2×2 k-point grid.

3. Results and discussion

3.1. Phase composition and crystal structure. All $LiGa_5O_8$-based samples synthesised presented in Table 1 show a pure cubic spinel structure (Fig. 1a). Only in the materials of nominal compositions $Li(Ga_{0.9}In_{0.1})_5O_8$ and $Li(Ga_{0.8}Al_{0.14}In_{0.06})_5O_8$ with relatively higher indium content, the traces of γ-$(Ga,In)O_3$ mixed oxide could be detected. Left- and right-side

shift of the Bragg's maxima of the In- and Al-substituted samples (see Fig. 1b) indicates successful and progressive incorporation of both these ions into the $LiGa_5O_8$ structure.

View Article Online
DOI: 10.1039/D6DT00337K

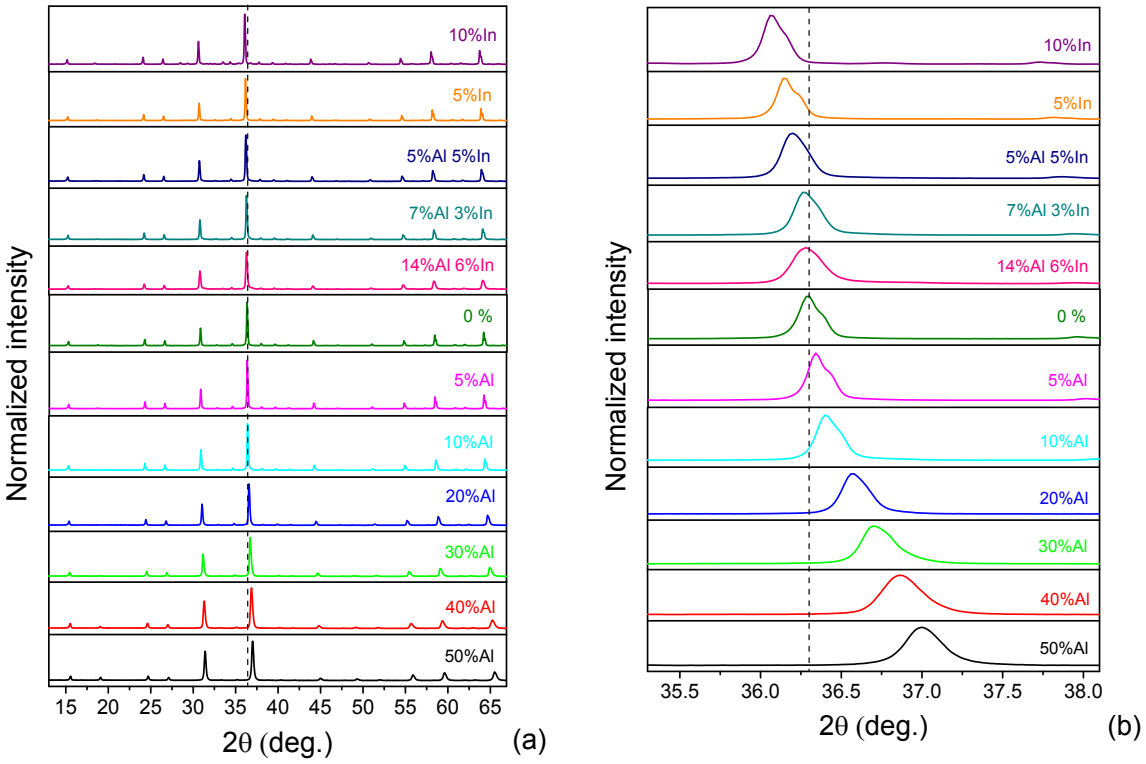

Fig. 1 Fragments of XRD patterns of the Cr-doped $LiGa_5O_8$-based materials. Vertical dashed lines serve as a guide for the eye, for tracking the changes in the position of Bragg's maxima due to a partial substitution of gallium ions with aluminium and/or indium species in $LiGa_5O_8$ structure.

More deep examination of experimental XRD profiles of the $Li(Ga_{1-x}Al_x)_5O_8$ series revealed significant and progressive peak broadening with increasing Al content (Fig. 1b), caused by a drastic increase of the microstrain values <ε> in these mixed spinel materials from 0.01-0.02 % for nominally pure $LiGa_5O_8$ and $x = 0.05$ sample to 0.19 – 0.24 % for the Al-richest samples with $x = 0.4$ and 0.5, as it was further derived by full profile Rietveld refinement. This is obviously caused by an increase in the dispersion of interplanar distances with increasing Al content in the $Li(Ga_{1-x}Al_x)_5O_8$ series.

To shed light on the peculiarities of cation substitution in the $LiGa_5O_8$ spinel structure, precise structural analysis was performed by full profile Rietveld refinement technique. As a starting model for the refinement, atomic positions in the prototype $LiFe_5O_8$ spinel structure derived from X-ray single crystal data of Tomas et al.[26] were used. After adjusting of the lattice parameters along with corrections instrumental sample shift, the atomic coordinates of and

displacement parameters (adp's) of atoms were refined. For the unsubstituted $LiGa_5O_8$:Cr material the excellent fit and very low residuals of $R_I = 0.0277$ and $R_P = 0.0407$ was obtained (see Table 2). In the case of $Li(Ga_{1-x}Al_x)_5O_8$:Cr series, structural refinement using different combinations of metal cations in the two non-equivalent Ga-sites showed that the better fit with the lowest residuals and physically reliable values of adp's (see Fig. S1 and Table 2) were achieved assuming mixed occupancy of the octahedral Ga1 position with Ga^{3+} and Al^{3+} ions, whereas the tetrahedral position of Ga2 atoms remains occupied mainly with gallium. In contrast, for the indium-substituted $Li(Ga_{0.95}In_{0.05})_5O_8$:Cr and $Li(Ga_{0.9}In_{0.1})_5O_8$:Cr samples, better results were achieved assuming that In^{3+} ions partially replace gallium in the Ga2 tetrahedral sites of the $LiGa_5O_8$ spinel structure (Table 2). This rather unexpected result was further corroborated by analysis of the obtained structural information, in particular, evolution of the average bond lengths inside two kinds of polyhedra *vs* substitution level in the $Li(Ga_{1-x}Al_x)_5O_8$ and $Li(Ga_{1-x}In_x)_5O_8$ spinel structures (see below). Structural refinement of the doubly substituted $Li(Ga_{0.9}Al_{0.05}In_{0.05})_5O_8$ and $Li(Ga_{0.9}Al_{0.07}In_{0.03})_5O_8$ materials using different combinations of metal cations in the two non-equivalent Ga-sites showed that the lowest residuals and physically reliable values of adp's were achieved when the octahedral Ga1 position in spinel structure is occupied with a mixture of Ga^{3+} and Al^{3+} ions, while the tetrahedral 8c site contains Ga^{3+} and In^{3+} species (see Fig. S1 and Table 2).

The refined structural parameters and atomic occupancy of nominally pure $LiGa_5O_8$, four representatives of Al- and In-substituted spinels and double substituted $Li(Ga_{0.9}Al_{0.05}In_{0.05})_5O_8$ material are summarised in Table 2.

$LiGa_5O_8$ belong to the $LiFe_5O_8$ type of structure - an 1:3 ordered variant of inverse spinel structure with gallium both in tetrahedral and octahedral sites and Li ions in octahedral environment, according to the notation $Ga_2(LiGa_3)O_8$. Fig. 2 shows polyhedral visualisation of crystal structure of $Li(Ga_{1-x-y}Al_xIn_y)_5O_8$ solid solutions, in which Al^{3+} and In^{3+} ions partially replace the Ga^{3+} ions in octahedral 12*b* and tetrahedral 8*c* sites, respectively. Both GaO_6 octahedra and GaO_4 tetrahedra in the $LiGa_5O_8$ structure are not regular, as it was reported in Refs.,[13,14] but considerably distorted both in the terms of variation of intrapolyhedral Ga-O distances (see Fig. 2, right panel) and the deviations of O-Ga-O bond angles from the ideal values of 90 and 109.47 degrees, respectively (see corresponding section below). In spite of six nearest Li-O distances in the $LiGa_5O_8$ structure are all equal, the LiO_6 octahedra are not fully regular due to the detectable deviation of O-Li-O bond angles from 90 degrees (see section below).

View Article Online
DOI: 10.1039/D6DT00337K

Table 2. Lattice parameters, fractional coordinates and displacement parameters of atoms in the structures of 0.5% Cr-doped $LiGa_5O_8$-based spinel materials (SG $P4_332$, $Z = 4$)

Atoms, sites	*x/a*	*y/b*	*z/c*	$B_{iso/eq}$, Å^2	Occupancy
$LiGa_5O_8$: a = 8.20421(5) Å; R_I = 0.0277, R_P = 0.0407					
Li, 4*b*	5/8	5/8	5/8	0.61(13)	*Li^+
Ga1, 12*b*	1/8	0.36562(3)	-*y* + 1/4	0.916(7)	1.002(2) Ga^{3+}
Ga2, 8*c*	-0.00360(4)	*x*	*x*	0.832(8)	1.001(1) Ga^{3+}
O1, 8*c*	0.3865(2)	*x*	*x*	0.95(4)	0.999(2) O^{2-}
O2, 24*e*	0.1200(2)	0.1286(1)	0.3854(1)	1.25(2)	0.999(2) O^{2-}
$Li(Ga_{0.95}Al_{0.05})_5O_8$: a = 8.19413(6) Å; R_I = 0.0260, R_P = 0.0501					
Li, 4*b*	5/8	5/8	5/8	0.9(2)	*Li^+
Ga1, 12*b*	1/8	0.36561(4)	-*y* + 1/4	1.21(1)	0.974(5) Ga^{3+} + 0.026(5) Al^{3+}
Ga2, 8*c*	-0.00412(4)	*x*	*x*	0.91(1)	1.001(5) Ga^{3+} + 0.001(5) Al^{3+}
O1, 8*c*	0.3878(2)	*x*	*x*	1.67(7)	0.999(2) O^{2-}
O2, 24*e*	0.1216(2)	0.1283(2)	0.3829(2)	1.28(4)	0.997(2) O^{2-}
$Li(Ga_{0.5}Al_{0.5})_5O_8$: a = 8.0569(2) Å; R_I = 0.0318, R_P = 0.0789					
Li, 4*b*	5/8	5/8	5/8	0.8(2)	*Li^+
Ga1, 12*b*	1/8	0.36855(8)	-*y* + 1/4	1.12(2)	0.203(2) Ga^{3+} + 0.797(2) Al^{3+}
Ga2, 8*c*	-0.00251(6)	*x*	*x*	1.346(9)	0.952(3) Ga^{3+} + 0.048(3) Al^{3+}
O1, 8*c*	0.3847(2)	*x*	*x*	2.30(7)	0.999(3) O^{2-}
O2, 24*e*	0.1091(2)	0.1311(1)	0.3870(2)	1.42(3)	1.000(2) O^{2-}
$Li(Ga_{0.95}In_{0.05})_5O_8$: a = 8.23558(6) Å; R_I = 0.0275, R_P = 0.0582					
Li, 4*b*	5/8	5/8	5/8	0.7(2)	*Li^+
Ga1, 12*b*	1/8	0.36583(4)	-*y* + 1/4	0.94(1)	1.000(6) Ga^{3+} + 0.000(6) In^{3+}
Ga2, 8*c*	-0.00304(5)	*x*	*x*	0.90(1)	0.931(6) Ga^{3+} + 0.069(6) In^{3+}
O1, 8*c*	0.3856(3)	*x*	*x*	1.50(7)	0.996(3) O^{2-}
O2, 24*e*	0.1150(2)	0.1270(2)	0.3878(2)	1.35(3)	0.998(2) O^{2-}
$Li(Ga_{0.9}Al_{0.05}In_{0.05})_5O_8$: a = 8.22835(8) Å; R_I = 0.0265, R_P = 0.0560					
Li, 4*b*	5/8	5/8	5/8	0.7(2)	*Li^+
Ga1, 12*b*	1/8	0.36580(4)	-*y* + 1/4	0.820(9)	0.960(6) Ga^{3+} + 0.040(6) Al^{3+}
Ga2, 8*c*	-0.00325(4)	*x*	*x*	0.932(10)	0.860(5) Ga^{3+} + 0.140(5) In^{3+}
O1, 8*c*	0.3898(2)	*x*	*x*	0.63(6)	0.998(3) O^{2-}
O2, 24*e*	0.1182(2)	0.1294(2)	0.3863(2)	1.22(2)	0.998(2) O^{2-}

* fixed at unity

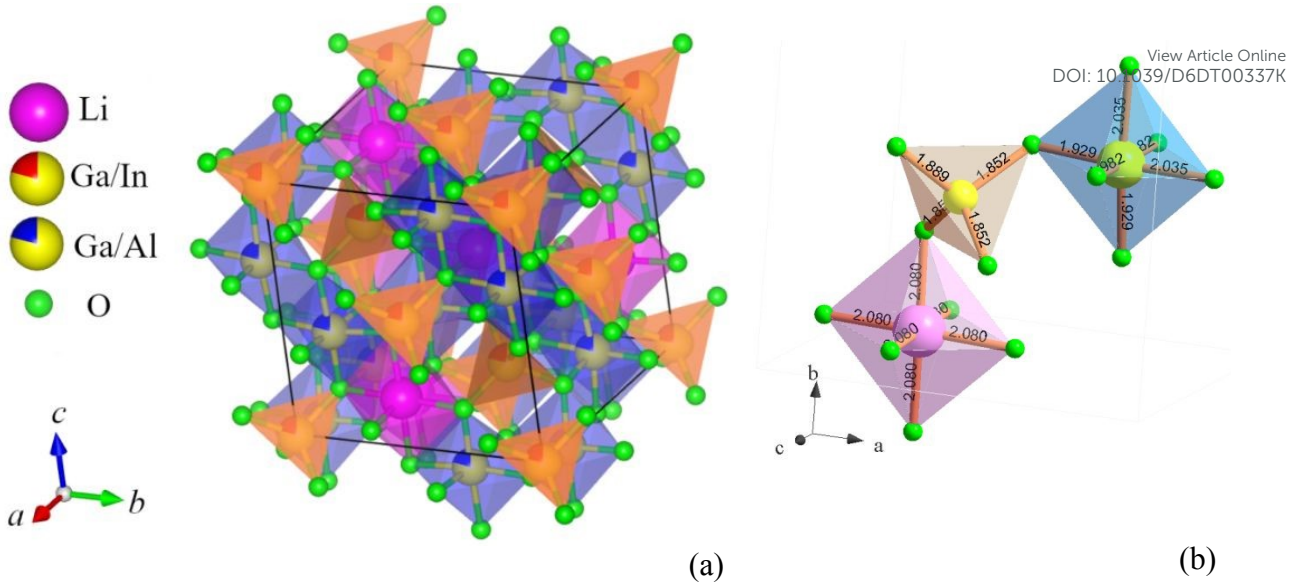

Fig. 2 Vesta plot of $Li(Ga_{1-x-y}Al_xIn_y)_5O_8$ crystal structure showing preferred location of substituting Al and In ions in octahedral Ga1 and tetrahedral Ga2 positions of the 1:3 ordered inverse spinel structure (a) and configuration of three types of coordination polyhedra in the parent $LiGa_5O_8$ structure (b).

The analysis of the structural results shows that the lattice parameters of both mixed spinel series demonstrate the expected opposite behaviour with an increase in the cation substitution level – a systematic linear decrease in $Li(Ga_{1-x}Al_x)_5O_8$ materials and clear increase in the case of $Li(Ga_{1-x}In_x)_5O_8$ samples (Fig. 3, left panel), which corresponds to the tabulated ionic radii of the Ga^{3+} ion of the host $LiGa_5O_8$ structure and the substituting Al^{3+} and In^{3+} species, respectively.[27] For the doubly substituted $Li(Ga_{1-x-y}Al_xIn_y)_5O_8$ samples, the lattice parameters lie between Al- and In-substituted series.

The peculiarities of cation substitution in the two investigated series can be noted when considering the nearest cation-oxygen environment in corresponding structures (Fig. 3, right panel). Increasing Al content in the $Li(Ga_{1-x}Al_x)_5O_8$ series mainly affects the average *M*-O distances within the $(Ga,M)O_6$ octahedra, which start to gradually decrease from x=0.1, while the average bond lengths inside $(Ga,M)O_4$ tetrahedra remain practically unchanged. In contrast, in the $Li(Ga_{1-x}In_x)_5O_8$ materials entering of In into the host $LiGa_5O_8$ structure causes pronounced increase in the average bond lengths inside the $(Ga,M)O_4$ tetrahedra without noticeable changes in the intraoctahedral distances. This observation confirms the above conclusion obtained from the Rietveld refinement that aluminium ions prefer to occupy octahedral 12*b* position in $Li(Ga_{1-x}Al_x)_5O_8$ structures, whereas large indium cations mainly occupy 8*c* Ga tetrahedral site in the $Li(Ga_{1-x}In_x)_5O_8$ structures.

View Article Online
DOI: 10.1039/D6DT00337K

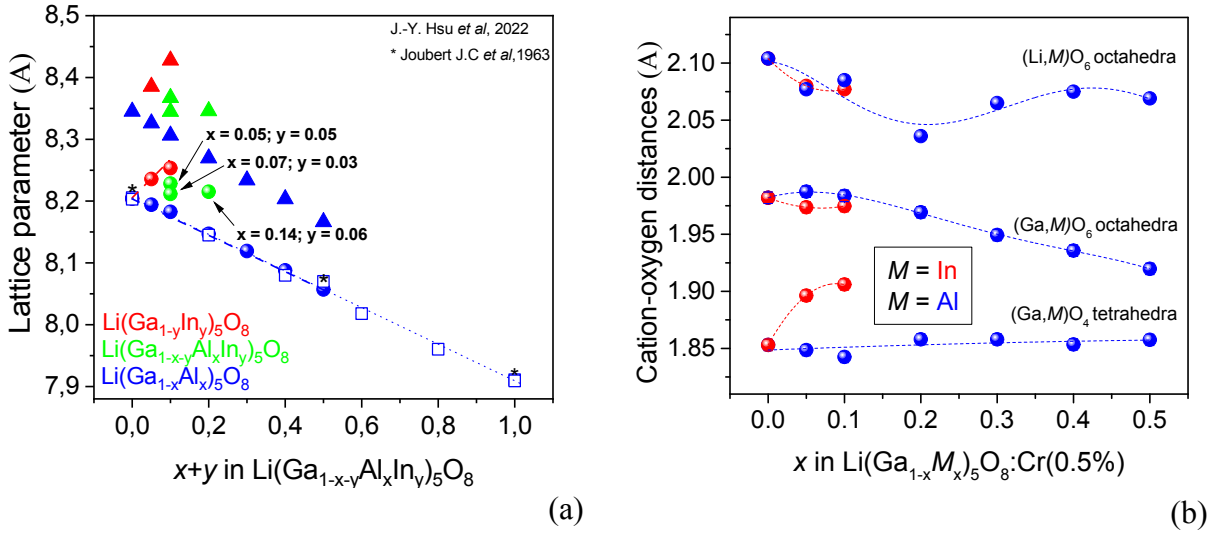

Fig. 3 Concentration dependence of the calculated (triangles) and experimental (circles) lattice parameters (a) and average Ga-O interatomic distances (b) in $Li(Ga_{1-x}Al_x)_5O_8$ and $Li(Ga_{1-x}In_x)_5O_8$ series (blue and red spheres, respectively). Open squares and the asterisks denote the lattice parameters taken from Refs.,[13,28] respectively. Dashed lines show polynomial fits for the eye guide.

Examination of the nearest environment of the Li ions in 4*b* site, which are surrounded by six equidistance oxygen ions, revealed a sudden discontinuity at x=0.2 against a background of a downward trend with increasing x in the $Li(Ga_{1-x}Al_x)_5O_8$ series. This observation can indicate that a partial inclusion of the smallest Al ions on the octahedral position of Li ions in 4*b* site could not be neglected. Similar phenomenon, *i.e.* mixed occupancy of octahedral 4*b* site with Li and Fe ions in the prototyping $LiFe_5O_8$ structure was reported in Tomas et al.[26] Unfortunately, negligible scattering factor of lithium ions does not allow to refine adequately a possible mixed occupancy of 4*b* site with different metal ions in $Li(Ga_{1-x}Al_x)_5O_8$ from the X-ray diffraction data.

Deeper analysis of structural parameters of the $Li(Ga_{1-x}Al_x)_5O_8$ series allows to reveal several interesting features in the concentration behaviour of the individual interatomic distances inside three different coordination polyhedra – tetrahedra GaO_4, and octahedra GaO_6 and LiO_6 (Fig. 4, green, red and blue symbols, respectively). All these distances show a detectable decreasing tendency due to overall lattice contraction $Li(Ga_{1-x}Al_x)_5O_8$ series and exhibit clear discontinuity between x=0.1 and 0.2. Three different Ga-O distances inside GaO_6 octahedra, after its initial approach at x=0.1, begin to progressively divergence with further increasing Al content. In contrast, two distinct distances within GaO_4 tetrahedra (one Ga-O1

View Article Online
DOI: 10.1039/D6DT00337K

and three Ga-O2) display a clear convergence behaviour after x=0.1, becoming practically equal at x=0.3 and 0.4 (see Fig. 4).

The observed deviations from the regular trends of Ga-O distances in GaO_6 octahedra and GaO_4 tetrahedra are manifested in the corresponding bond length distortion parameters calculated according to Sasaki et al.[29] as

$$\Delta = \frac{1}{n}\sum \left(\frac{l_i - l_{CN}}{l_{CN}}\right)^2 \times 10^3, \quad (1)$$

where li and l_{CN} are the individual and average interatomic distances in polyhedra with corresponding coordination number, and n is the number of bonds. Clear extrema in the bond length distortion – a minimum for GaO_6 octahedra and the maximum for GaO_4 tetrahedra (Fig. 4, right top panel) – reflect the complex character of cation substitution in $Li(Ga_{1-x}Al_x)_5O_8$ series. Since the six Li-O distances inside LiO_6 octahedra are equal due to the symmetry of 4*b* site, there is no bond length distortion (Δ= 0). However, LiO_6 octahedra cannot be considered as regular due to the deviation of bond angles inside the octahedra from 90 degrees. Bond angle distortion (variance) in coordination polyhedra, σ, can be calculated similarly to bond length distortion: $\sigma = 1/n\Sigma((\varphi-\varphi_i)/\varphi_i)^2$. It stands as a measure of deviation of the actual bond angle φ from the ideal values φ_i for the corresponding polyhedra (90° for octahedra and 109.47° for tetrahedra). Evolution of calculated values for three distinguish polyhedra in $Li(Ga_{1-x}Al_x)_5O_8$ series is presented on the right bottom panel of Fig. 4. In the terms of bond angle variance σ, LiO_6 octahedra with six equal Li-O internal distances are considerably distorted and the uneven its increasing evolution *vs* Al content with a noticeable deflection at x=0.1 reflects complex scenario of cation substitution in the $Li(Ga_{1-x}Al_x)_5O_8$ series. Bond angle variance in GaO_6 octahedra and GaO_4 tetrahedra depends weakly on the $Li(Ga_{1-x}Al_x)_5O_8$ composition, in contrast to bond length distortion showing clear opposite extrema at x=0.1 (Fig. 4, right panel).

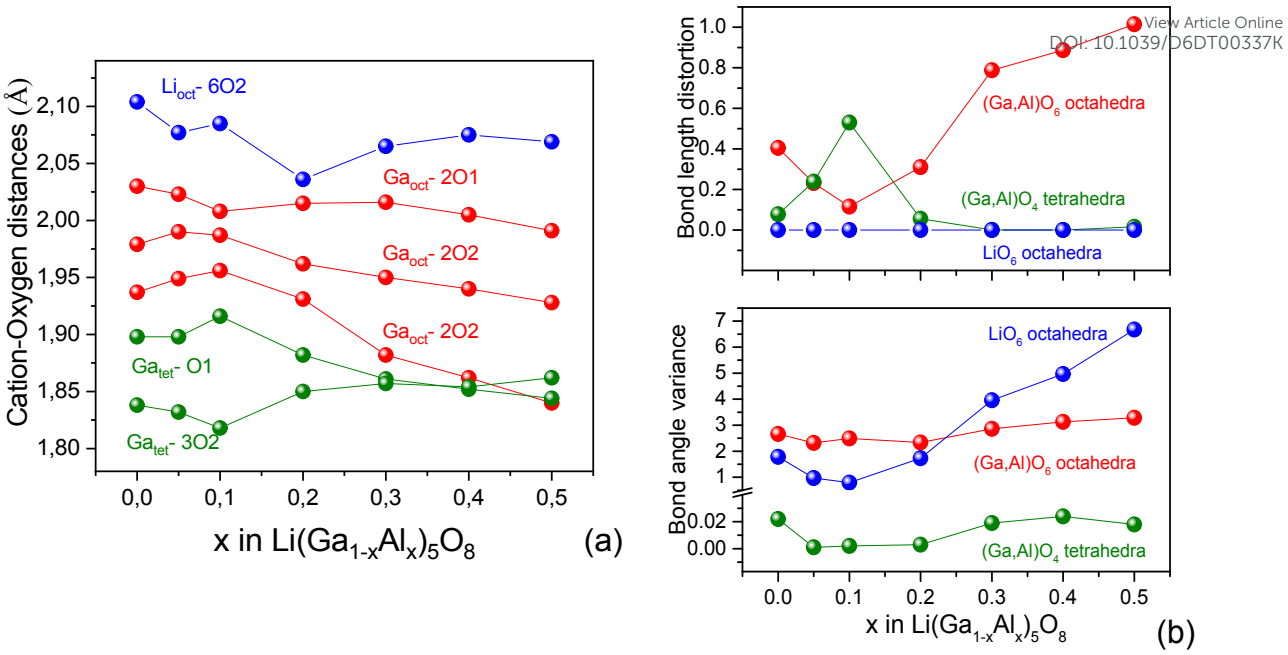

Fig. 4 Concentration evolution of nearest cation-oxygen distances (a) and bond length distortion in tetrahedral and two octahedral positions of metal ions (b) in the $Li(Ga_{1-x}Al_x)_5O_8$ series.

XRD examination of the same samples, annealed in a high vacuum at 1000 °C for 2 hours, revealed no detectable changes in the phase compositions and crystal structure parameters of the studied materials. Illustrative pictures from full profile Rietveld refinement proving phase purity and crystal structure of the $Li(Ga_{1-x}Al_x)_5O_8$, and $Li(Ga_{1-x}In_x)_5O_8$ $Li(Ga_{0.9}Al_{0.05}In_{0.05})_5O_8$ spinel materials after its reducing annealing are presented in Fig. S2. Refined structural parameters of these samples practically do not differ from the initial air annealed materials and show very similar concentration behaviour with increasing cation substitution level in $Li(Ga_{1-x}Al_x)_5O_8$ and $Li(Ga_{1-x}In_x)_5O_8$ series (see Fig. S3).

3.2. Microstructure and elemental composition. SEM imaging of the studied samples testifies that they have a strongly agglomerated microstructure, as shown in Fig. 5. It is noteworthy that the non-modified $LiGa_5O_8$ and the In-containing $Li(Ga_{0.95}In_{0.05})_5O_8$ samples have a typical size of the microcrystalline grains of ≥ 1 μm, while the Al-containing samples have smaller grains of up to 0.5 μm or even smaller for the $Li(Ga_{0.5}Al_{0.5})_5O_8$ sample.

EDX elemental analysis and mapping (see Fig. 6) confirm a uniform distribution of Ga, Al and In elements within the grains of the single-phase samples. At the same time, the Cr distribution in the maps is barely noticeable, obviously because of its low content (0.5 at.% with respect to Li), while its presence has been confirmed by a quantitative analysis of EDX spectra.

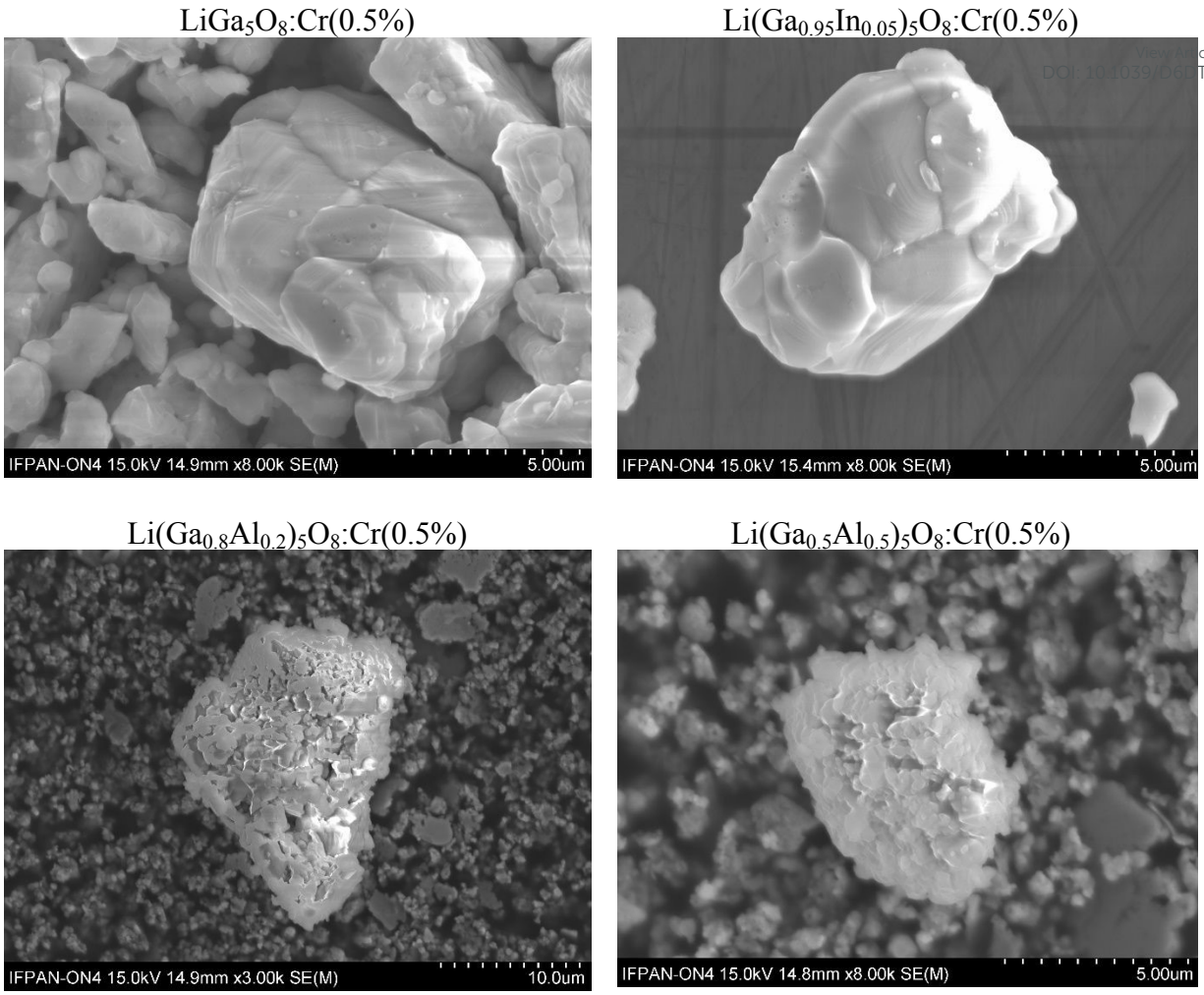

Fig. 5 High-resolution SEM images of the selected samples studied.

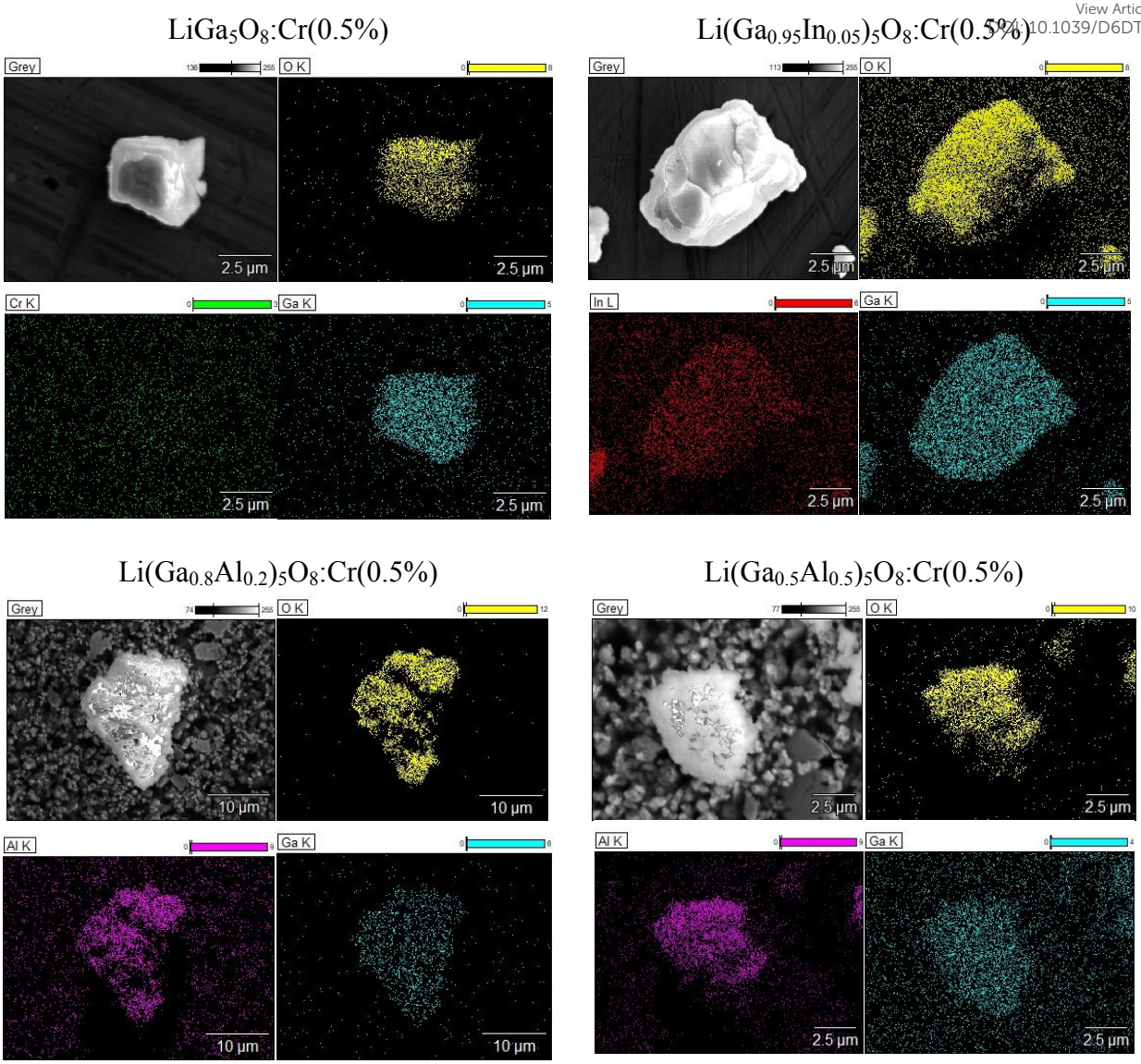

Fig. 6 EDX maps of the selected samples studied.

3.3. DFT Calculations. The calculated total energies E for all sets of $Li(Ga_{1-x}Al_x)_5O_8$ supercells are presented in Fig. 7. For each x value, the origin of the energy scale is chosen at the calculated E value of the lowest-energy structure. For each x, 10 structures were created with random location of Al over Ga positions, with Al_{Ga} randomly distributed between octahedral and tetrahedral cationic sites (see section 3.1 for details). The number of Al_{Ga} in tetrahedral positions is shown in Fig. 7 for each energy level corresponding to one such structure.

View Article Online
DOI: 10.1039/D6DT00337K

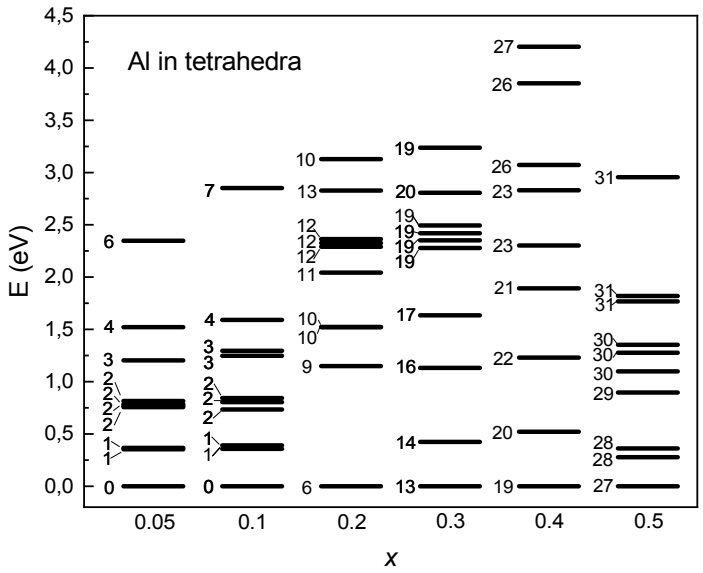

Fig. 7 Calculated total energies of $Li(Ga_{1-x}Al_x)_5O_8$ supercells with varying atomic structures grouped by the same x. Number of Al_{Ga} substitutions occupying tetrahedral sites are indicated for each supercell.

As Fig. 7 clearly shows, the more Al_{Ga} there is in tetrahedral positions in the structure, the greater its calculated total energy, and this trend is observed for all x values considered in calculations. Analysing the data presented in Fig. 7, it can be approximately assumed that when one additional Al_{Ga} cation is placed in any tetrahedral position of the lattice while maintaining the total amount of Al_{Ga} (*i.e.*, the value of x), the total energy of the structure increases by an average of 0.5–1 eV. From this fact, we can conclude that, regardless of the value of x, the most energetically favourable structures of $Li(Ga_{1-x}Al_x)_5O_8$ (x from 0 to 0.5) will be those in which all Al_{Ga} are in octahedral positions of the lattice.

As established from experimental results (see 3.1 section), Al_{Ga} substitutions preferentially occur at octahedral Ga sites. Our calculations definitely confirm this suggestion.

View Article Online
DOI: 10.1039/D6DT00337K

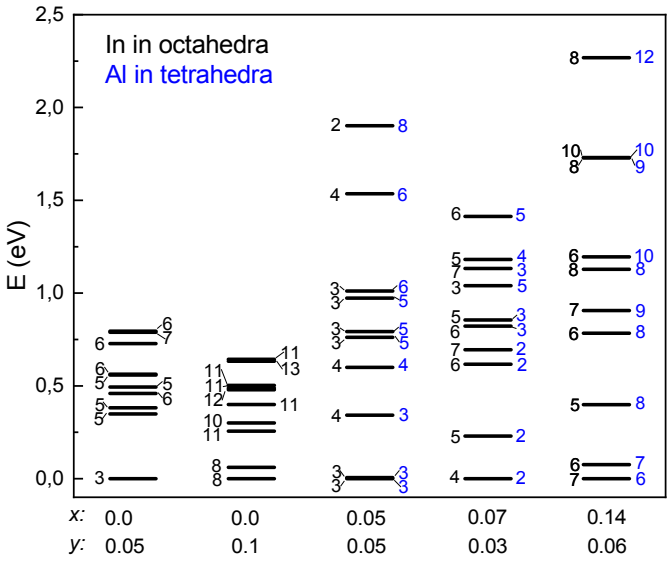

Fig. 8 Calculated total energies of $Li(Ga_{1-x-y}Al_xIn_y)_5O_8$ supercells with varying atomic structures grouped by the same *x* and *y*. Number of In_{Ga} in octahedral sites are indicated by black numbers, Al_{Ga} in tetrahedral sites – by blue ones.

At the same time, from experimental results it was suggested that In_{Ga} substitutions preferentially occupy octahedral Ga sites (see 3.1 section). This conclusion is also confirmed by our calculations. As can be seen in Fig. 8, the greater the number of In_{Ga} in octahedral sites in the structure, the higher its energy.

Taking into account the above results, the optical spectra calculations were performed for $Li(Ga_{1-x-y}Al_xIn_y)_5O_8$ supercells in which Al_{Ga} were situated only in octahedral positions, and In_{Ga} in tetrahedral ones. The lattice parameters of $Li(Ga_{1-x-y}Al_xIn_y)_5O_8$ obtained from DFT geometry optimizations of the supercells with the lowest-energy structures, in which Al_{Ga} randomly occupy octahedral, and In_{Ga} tetrahedral positions are presented in Fig. 3 (see 3.1 section) and also listed in Table S2. Although DFT-based optimizations usually slightly overestimate the unit cell volumes (and corresponding lattice constants) our calculations clearly reproduce the experimentally observed trends obtained for synthesised set of $Li(Ga_{1-x-y}Al_xIn_y)_5O_8$ samples.

Using calculations of the optical spectra of the lowest-energy $Li(Ga_{1-x-y}Al_xIn_y)_5O_8$ structures, we evaluated the trends in the crystal band gaps depending on the cation composition of the compound.

Dependencies of the calculated absorption spectra of $Li(Ga_{1-x-y}Al_xIn_y)_5O_8$ alloys on the values of *x* and *y* are shown in Fig. S5. From these data, we estimated the energies at which the

View Article Online
DOI: 10.1039/D5DT00337K

absorption coefficient of $Li(Ga_{1-x-y}Al_xIn_y)_5O_8$ alloy with specific x and y reaches the value of ~10^4 cm^{-1}, which has a pure $LiGa_5O_8$ crystal at energy of 4.9 eV (as it will be shown in the next section, this energy may reflect the onset of excitonic or band-to-band PL excitation). Using these energy points, we approximately estimate the shifts of the spectra of the alloys relative to the pure crystal. Although the spectra were obtained in approximate calculations, such shifts obviously have to correlate with changes in the energy gaps E_g of $Li(Ga_{1-x-y}Al_xIn_y)_5O_8$ compounds depending on the cation content.

If we presumably approximate the value of E_g of pure $LiGa_5O_8$ crystal as 4.9 eV (the actual value probably may be 0.2-0.5 eV higher),[30] then according to the above analysis of the calculation results, the trends in the energy gaps should be as shown in Fig. 9.

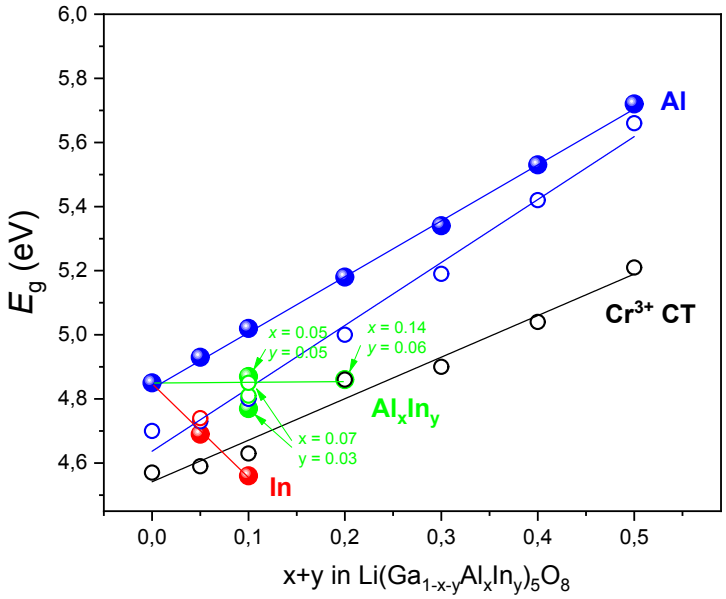

Fig. 9 Trends of band gap energies of $Li(Ga_{1-x-y}Al_xIn_y)_5O_8$ alloys estimated from the calculated optical absorption spectra (solid symbols), and those estimated experimentally from the photoluminescence excitation spectra (open symbols) with corresponding linear fittings.

As Fig. 9 shows, doping with 50% of Al increases the E_g value of $LiGa_5O_8$ by almost 1 eV. Indium doping, on the contrary, reduces the band gap, and this reduction has more pronounced concentration dependence: 10% of Al in the alloy increases its *Eg* by only 0.17 eV, while 10% of In reduces it by 0.30 eV. In addition, as can be seen from the figure (see green dots), simultaneous doping with Al and In (in concentrations of 5% Al + 5% In and 14% Al + 6% In) practically does not change the band gap of $LiGa_5O_8$ crystal. There is clear correlation between band gap energy and lattice parameters (unit cell volume) of $Li(Ga_{1-x-y}Al_xIn_y)_5O_8$ solid

solutions: the smaller the unit cell volume in $Li(Ga_{1-x}Al_x)_5O_8$ series - the wider the band gap, and the larger the volume of unit cell in $Li(Ga_{1-x}In_x)_5O_8$ series - the narrower band gap (compare Fig. 3a and Fig. 9). Similar effect has recently been observed for the aluminium and indium substituted β-Ga_2O_3-based solid solutions with monoclinic structure.[25]

Thus, the results of our calculations show the possibility of band gap engineering of $Li(Ga_{1-x-y}Al_xIn_y)_5O_8$ compounds: the E_g value can be significantly increased by Al doping, decreased by In doping, and maintained at the same level by co-doping Al and In in a certain proportion.

3.4. Photoluminescence. The room-temperature PL and corresponding PLE spectra of the studied samples are shown in Fig. 10 and Fig. 11. These results reveal the characteristic spectra of Cr^{3+} centres in octahedral coordination.[31] In particular, the excitation bands at about 600 and 400 nm are caused by the spin-allowed $^4A_2 \rightarrow {}^4T_2$ (^4F) and $^4A_2 \rightarrow {}^4T_1$ (^4F) transitions of Cr^{3+}, respectively, while the third excitation band at about 300 nm is related most probably to the $^4A_2 \rightarrow {}^4T_2$ (^4P) transition of Cr^{3+} and/or the charge transfer (CT) transitions with the participation of Cr^{3+} (see *e.g* Stasiv at al).[11] Above these excitation bands, an edge-like excitation caused by the band-to-band transitions in the host lattice is observed. It is noteworthy that upon partial substitution of gallium by aluminium, the 600 and 400 nm excitation bands shift towards higher energies, and conversely, when Ga is replaced by In, a red shift of these bands is observed. This behaviour is consistent with the results reported previously[32, 13, 11] and arises from the alteration in crystal field strength experienced by Cr^{3+} ions due to the replacement of Ga ions by Al or In. A larger shift of the edge-like and the CT excitation bands is obviously caused by the alteration in the band gap of the host lattice (see also Fig. 9 and Fig. S7). As one can see from Fig. 9, the shift of the excitation edge related to band-to-band transitions (which characterises the shift in the material band gap) is well consistent with that estimated from the calculated optical absorption spectra.

The photoluminescence spectra of the studied samples at room temperature (Fig. 11a) do not reveal any significant difference for the studied compositions of the host lattice. The PL spectrum is featured by a narrow line at about 718 nm (deviating within 2 nm depending on the Al/In content) caused by the zero-phonon line (spin-forbidden $^2E \rightarrow {}^4A_2$ transition of Cr^{3+}) and vibronic sidebands originating from the same transition (see *e.g*. Hsu et al.).[13] The replacement of Ga by up to 50% of Al does not cause any noticeable changes in the room-temperature PL spectrum, while adding of 5% of In increases somewhat a relative intensity of the vibronic sidebands around the 718 nm line. All the studied samples demonstrate the quantum efficiency

(QE) of photoluminescence of about 50% except the samples with 5 and 10% of Al, for which a lower QE was revealed (Fig. 11b).

View Article Online
DOI: 10.1039/D6DT00337K

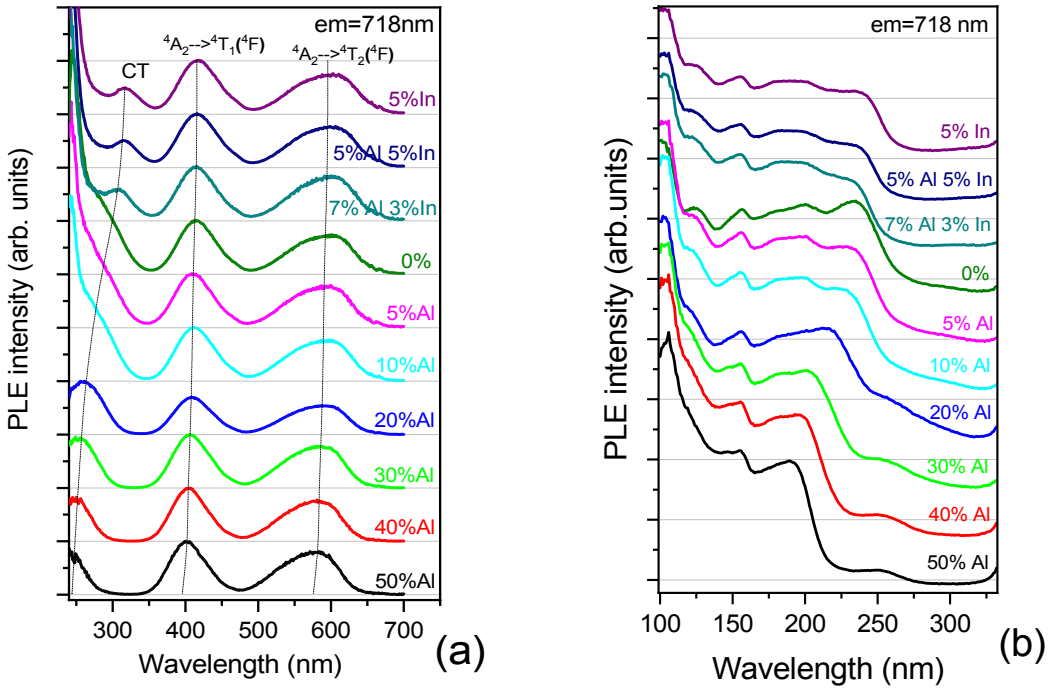

Fig. 10 Room-temperature photoluminescence excitation (PLE) spectra of the studied samples measured in UV-vis (a) and VUV-UV (b) ranges when registered at 718 nm. The dotted lines demonstrating the peak positions are only a guide for the eyes.

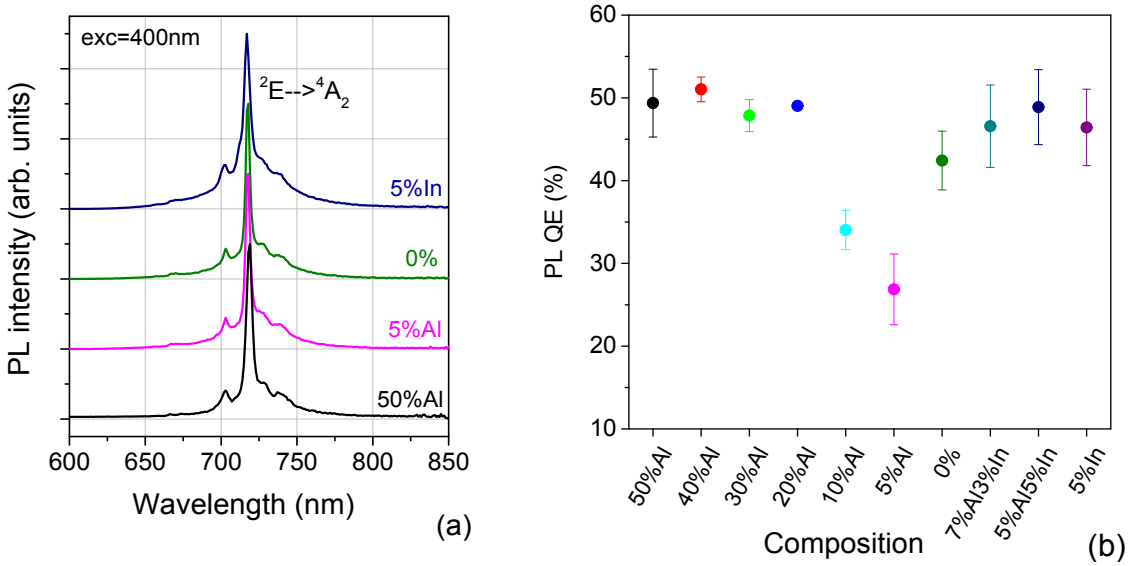

Fig. 11 Room-temperature photoluminescence (PL) spectra (a) and PL quantum efficiency (QE) (b) of the studied samples at 400 nm excitation.

View Article Online
DOI: 10.1039/D6DT00337K

3.5. Temperature dependence of photoluminescence. The temperature evolution of the photoluminescence spectra of the studied samples is shown in Fig. 12. As it is seen from the figure, the narrow-line emission at 718 nm is superimposed on the broadband emission, which stretches from 600 to about 850 nm. This broadband emission, caused most likely by the spin-allowed $^4T_2(^4F) \rightarrow {}^4A_2$ transition of Cr^{3+}, became apparent at elevated temperatures. As seen from the Fig. 12, the narrow-line emission at 718 nm is the only one present at temperatures much below room temperature and decreases in intensity as temperature increases. Above 200 K, the broadband emission appears and grows, reaching its maximum at about 400 K, while the narrow-line emission disappears. The broadband emission quenches in turn at higher temperatures. Similar temperature behaviour of the $^2E \rightarrow {}^4A_2$ and $^4T_2(^4F) \rightarrow {}^4A_2$ emissions of Cr^{3+} has previously been reported, *e.g.* for Ga_2O_3:Cr^{3+}, and is typical for Cr^{3+} centres in an intermediate crystal field strength when the ^2E and $^4T_2(^4F)$ emitting levels are in thermal equilibrium.[33]

Temperature dependences of the overall PL intensity of the studied samples are shown in Fig. 13, and corresponding quenching parameters are collected in Table 3. It should be mentioned that the measured temperature dependence of the PL intensity cannot be adequately fitted by the simplest quenching process:

$$I(T) = \frac{I(0)}{1+A\exp\left(-\frac{\Delta E}{kT}\right)}, \quad (2)$$

where $I(0)$ is the emission intensity at zero temperature, ΔE is the activation energy of non-radiative transitions, and A is the ratio of the non-radiative transition probability to the radiative transition probability. To get more precise fitting of the experimental data, at list a two-step quenching model in accordance with Zhydachevskyy et al.[34] should be applied:

$$I(T) = \frac{I(0)}{1+A_1\exp\left(-\frac{\Delta E_1}{kT}\right)+A_2\exp\left(-\frac{\Delta E_2}{kT}\right)}, \quad (3)$$

where ΔE_1 and ΔE_2 are the activation energies of two competing non-radiative pathways with corresponding parameters, A_1 and A_2, related to the strength of the quenching processes. The presence of two competition quenching mechanisms seems obvious owing to at least two quenching processes observed experimentally, in particular, (i) the quenching of the narrow-line emission from ^2E level by thermal population of the $^4T_2(^4F)$ level of Cr^{3+}, and (ii) the thermal quenching of the emission from $^4T_2(^4F)$ level itself. Besides, the possibility of multiple types of Cr^{3+} centres in the studied spinel host cannot be excluded as well.

View Article Online
DOI: 10.1039/D6DT00337K

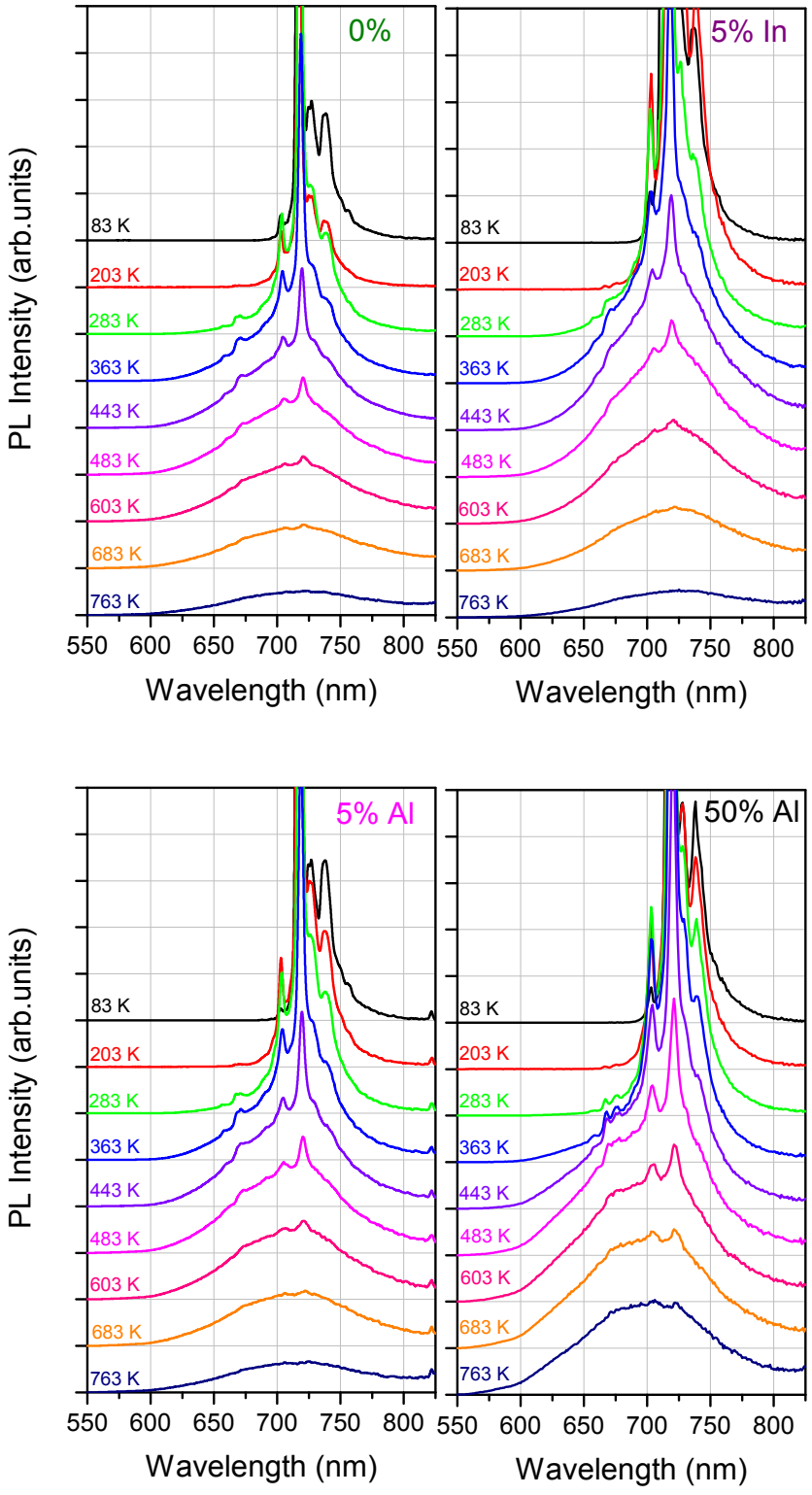

Fig. 12 Temperature evolution of PL spectra of selected samples.

View Article Online
DOI: 10.1039/D6DT00337K

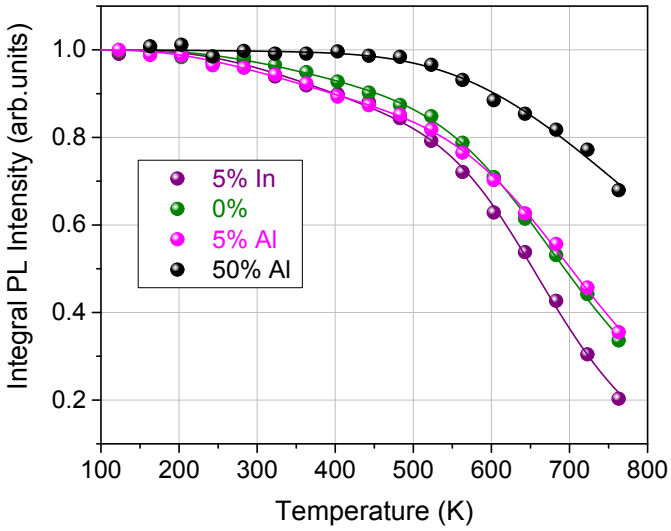

Fig. 13 Temperature dependence of PL intensity of selected samples. Solid lines represent the fitting by the eqn (3).

Table 3. Parameters of fits obtained from the temperature dependence of the emission intensity eqn (3) for the studied $Li(Ga_{1-x-y}Al_xIn_y)_5O_8:Cr^{3+}$ compounds.

Sample composition	ΔE_1, eV	ΔE_2, eV	A_1	A_2	$T_{1/2}$, K	ΔE*, eV[13]
5% In	0.097 ± 0.001	0.61 ± 0.04	1.87 ± 0.7	3.4e3 ± 2.5e3	653	–
0% Al	0.094 ± 0.017	0.49 ± 0.03	1.13 ± 0.51	3.1e3 ± 1.6e3	694	0.123 ± 0.01
5% Al	0.078 ± 0.009	0.52 ± 0.03	1.08 ± 0.26	4.2e3 ± 2.2e3	702	–
50% Al	0.055 ± 0.19	0.35 ± 0.05	0.02 ± 0.15	1.0e2 ± 0.8e2	>800	–
60% Al	–	–	–	–	–	0.123 ± 0.004
100% Al	–	–	–	–	–	0.112 ± 0.04

* the ΔE value obtained from fitting by eqn (2) in Hsu et al.[13]

As it is seen from Fig. 13 and Table 3, the quenching temperature $T_{1/2}$ decreases with the replacement of Ga by In, and increases when Ga is replaced by Al. It should be noted that the activation energy ΔE estimated in Hsu et al.[13] using the fitting by eqn (2) in much narrower temperature range is in the middle of the ΔE_1 and ΔE_2 values obtained by us.

To get insight into the possibility of multiple Cr^{3+} centres formation in the studied compounds, a zero-phonon line (ZPL) emission originating from the $^2E \rightarrow {}^4A_2$ transition in the octahedrally-coordinated Cr^{3+} has been measured at liquid helium temperature. It is known that

View Article Online
DOI: 10.1039/D5DT00337K

this emission is very sensitive to the local structure of Cr^{3+} environment and their splitting (R-lines) can be used as a measure of the distortion of the CrO_6 octahedron.[35] Recently, it was shown that in the monoclinic $(Ga_{1-y}Al_y)_2O_3$ and $(Ga_{1-x}In_x)_2O_3$ solid solutions doped with Cr^{3+}, different distinct Cr^{3+} centres can be recognised in ZPL, which were attributed to the Al-, Ga- and In-centred octahedra in this alloyed structure.[11] So it is of interest to check this for the spinel $Li(Ga_{1-x-y}Al_xIn_y)_5O_8:Cr^{3+}$ compounds studied here. As it is seen form Fig. 14, the $LiGa_5O_8$:Cr (0% Al) sample is featured by a single and narrow ZPL at 716.7 nm. When Al is added, the same ZPL is observed, however, it gradually broadens and shifts towards longer wavelength as Al content increases. When In is added, the same ZPL also broadens, however, it shifts in the opposite direction. It is also evident that for the In-containing samples, the line has got two additional components in the long- and short-wavelength sides of the main ZPL. Here, it should be noted that the additional ZPLs observed for the In-containing samples are not related to the second component (R_2-line) of zero-phonon emission from the possibly split ^2E level. Fig. 15 demonstrates that the thermally populated R_2 component appears at the short-wavelength side of R_1 at temperatures above 60 K. It is noteworthy that the R_2 line for the In-containing compounds also has a multiple structure like R_1. It is also noteworthy that the ^2E level splitting (R_2-R_1 distance) for Cr^{3+} in $LiGa_5O_8$ is about 34.6 meV, which is twice as large as 18.2 meV for β-$Ga_2O_3:Cr^{3+}$,[33] suggesting a larger distortion of Cr-centred octahedra (meaning GaO_6 octahedra) in $LiGa_5O_8$ than in β-Ga_2O_3. It is also worth noting that the ^2E level splitting in $LiGa_5O_8$ increases gradually with increasing Al and In content (Fig. 15b), which is consistent with the bond length distortion in Ga octahedral positions presented in Fig. 4b.

View Article Online
DOI: 10.1039/D6DT00337K

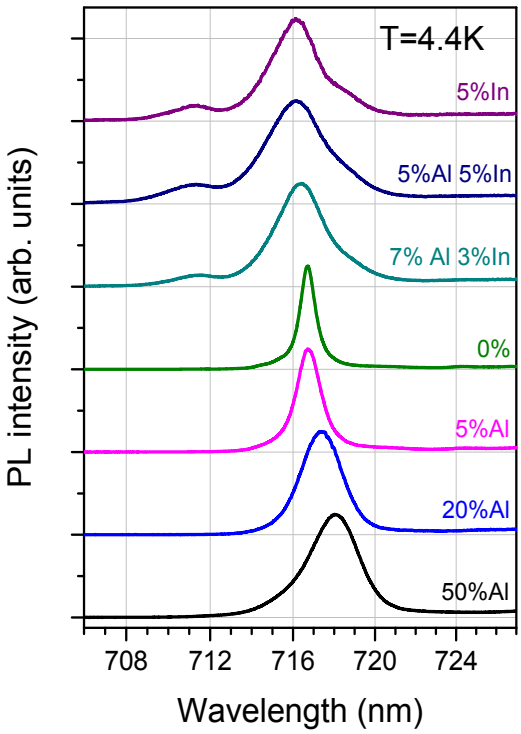

Fig. 14 High-resolution Cr^{3+} ZPL (R_1-line) emission spectra for the studied samples measured at $T = 4.4$ K.

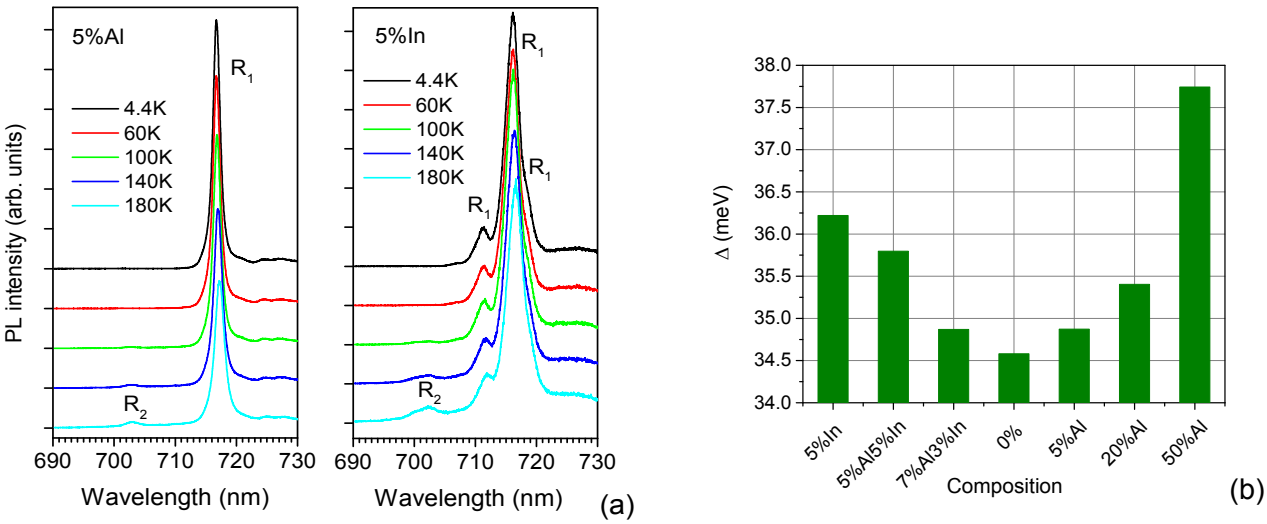

Fig. 15 Temperature evolution of Cr^{3+} ZPL emission spectra of the 5% Al and 5% In samples (a), and the splitting of ^2E level (R_2-R_1) of selected samples (b).

3.6. Thermoluminescence after UV exposure. All the studied samples, after UV exposure to the CT band at about 270-310 nm (see Fig. 10), were revealed to possess quite

efficient thermoluminescence below and above room temperature. Analysis of the TSL glow curves after UV exposure at a liquid nitrogen temperature, presented in Fig. 16a, reveals the following peculiarities. The thermoluminescence of pristine (non-modified by Al or In) $LiGa_5O_8$:Cr below and above room temperature is determined by the four main TSL peaks (marked as I, II, III and IV) with the peak maxima at about 120, 210, 350 and 500 K, respectively. Similar TSL peaks III and IV above room temperature were observed previously also for $LiGa_5O_8$:Pr^{3+}[3] $LiGa_5O_8$:Bi^{3+}[36] and $LiGa_5O_8$:Tb^{3+}[1] synthesised by a similar high-temperature solid-state reaction method. This similarity suggests that these TSL peaks are related to the same kind of intrinsic point defects, at least when the material is synthesised in air by the solid-state method.

It is noteworthy that all samples modified by Al and/or In reveal a similar TSL structure, however the position of the TSL peaks and their intensity ratios change. In particular, the position of all the TSL peaks shifts towards higher temperatures as Al content increases, and vice versa, the TSL peaks move towards lower temperatures when the host is modified by In that is consistent with the results observed previously for γ-$(Ga_{1-x-y}Al_xIn_y)_2O_3$.[11] Additionally, as Al replaces Ga, the intensity ratio of the first two peaks (I and II) to the third and fourth peaks (III and IV) increases significantly.

The temperature range starting from the room temperature to at least up to 100 °C (~374 K), which determines the room-temperature persistent luminescence, is marked in Fig. 16a. In such a way it is obvious that the room-temperature persistent luminescence of $LiGa_5O_8$:Cr and compounds with small amounts of Al and In will be determined by TSL peaks III and IV, while, for compounds with larger amounts of Al, it will be determined already by peaks I and II. A precise comparison of the corresponding relative TSL intensities for different samples in this temperature range is shown in Fig. 16b.

It is also evident that simultaneously with changing the TSL peaks position, the modification of the $LiGa_5O_8$ host by the addition of Al and/or In makes the TSL peaks broader. The TSL peak broadening means an expansion of the set of trap depths caused by local structure disorder introduced by the partial replacement of Ga atoms with Al and/or In, see Chang et al.[12] Assuming all other conditions (position of the peak and their intensity) are equal, the broadening of the TSL peaks themselves should result in more prolonged persistent luminescence of the material.

View Article Online
DOI: 10.1039/D6DT00337K

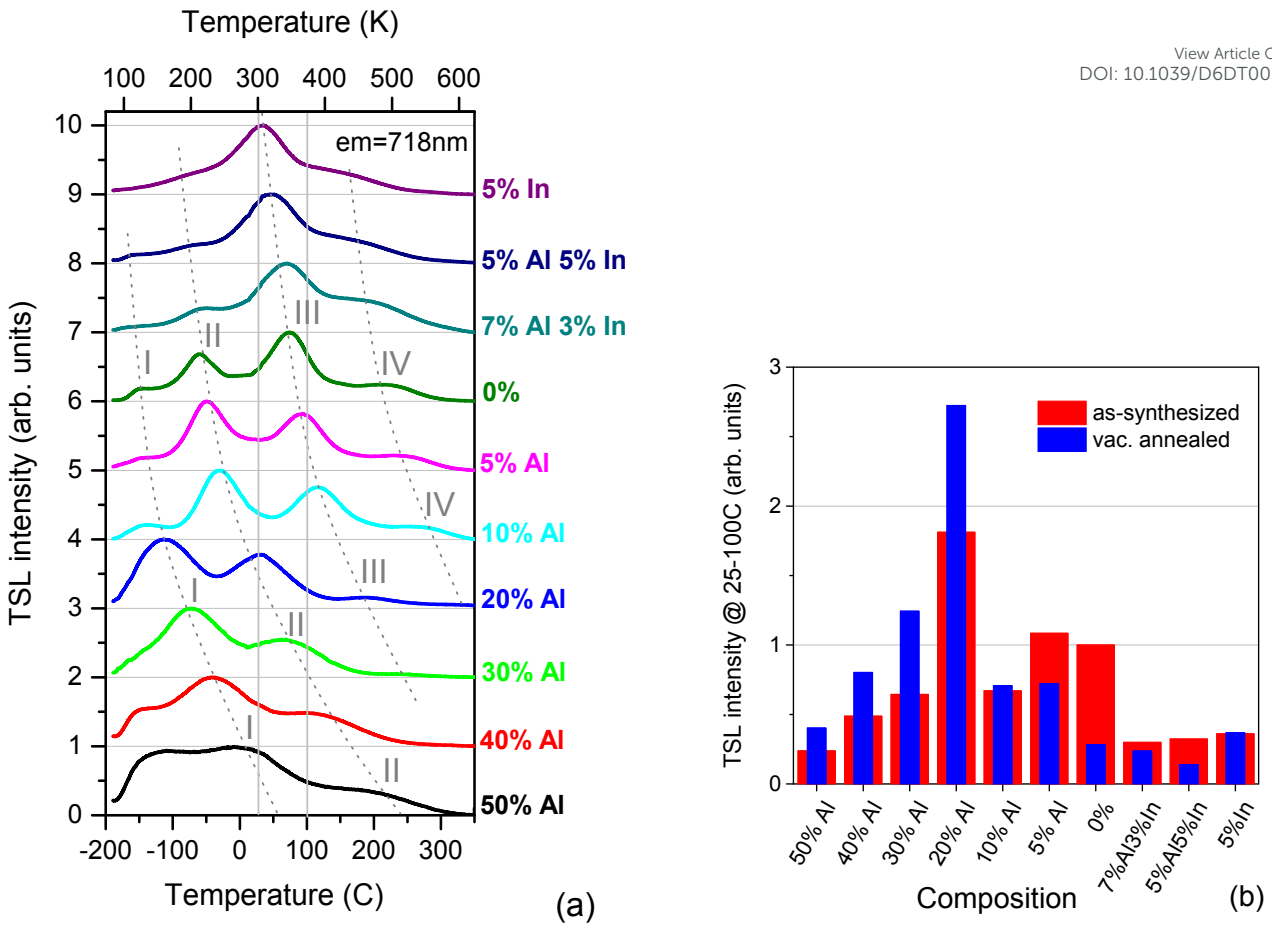

Fig. 16 Thermally stimulated luminescence (TSL) curves of the as-synthesised samples registered at 718 nm after UV (270-310 nm) exposure at a liquid nitrogen temperature (a); and corresponding relative TSL intensities integrated in the temperature range from 25 to 100 °C for different (as-synthesised and annealed in vacuum) samples as a function of their composition (b). Heating rate 1 C/s. The dotted lines demonstrating the peak positions are only a guide for the eyes.

*3.6.1. Effect of reducing annealing***.** Based on the belief that the radiation storage properties of the studied materials are caused by the oxygen-related intrinsic point defects (oxygen vacancies and interstitials), as reported by Jia et al.[9] , one can expect noticeable changes in TSL after the reducing thermal treatment of the materials synthesised in an oxidizing environment (*i.e.*, in air). Therefore, it is of interest to follow the changes caused by the high-temperature annealing of the studied materials in a vacuum. The TSL curves of the samples after such annealing, compared to the as-synthesised samples, are shown in Fig. S6. As one can see from Fig. S6, the reducing annealing does not change the TSL structure; however, the relative and absolute intensity of certain peaks does change. Specifically, the intensity of peaks III and IV is suppressed in all the studied samples, while peaks I and II usually increase, especially in the samples with a higher Al content. The increase in peaks I and II after annealing

the samples with higher Al content is undoubtedly beneficial and should enhance their room-temperature persistent luminescence. The relative TSL intensities in the temperature range of 25-100 °C of the annealed samples are also shown in Fig. 16b. In such a way, the highest TSL intensity at 25-100 °C is observed for the 20% Al sample annealed in vacuum, which reveals a threefold enhancement compared to the pristine $LiGa_5O_8$:Cr (0% Al) sample synthesised in air.

3.7. Persistent luminescence. After UV exposure to the CT band at about 270-310 nm, in the same way as TSL, the studied samples show an afterglow occurring in the deep-red spectral range corresponding to the Cr^{3+} emission in the materials. It should be noted that after exposure to visible light, including the 400 nm band, the afterglow is negligible. Fig. 17 compares the room-temperature afterglow of selected samples after the UV exposure. These results show good agreement with the TSL results presented above. In particular, samples containing 20% and 30% of Al reveal an enhanced PersL intensity compared to the pristine $LiGa_5O_8$:Cr (0% Al) sample, from which the 20% Al sample annealed in vacuum exhibits the highest PersL intensity.

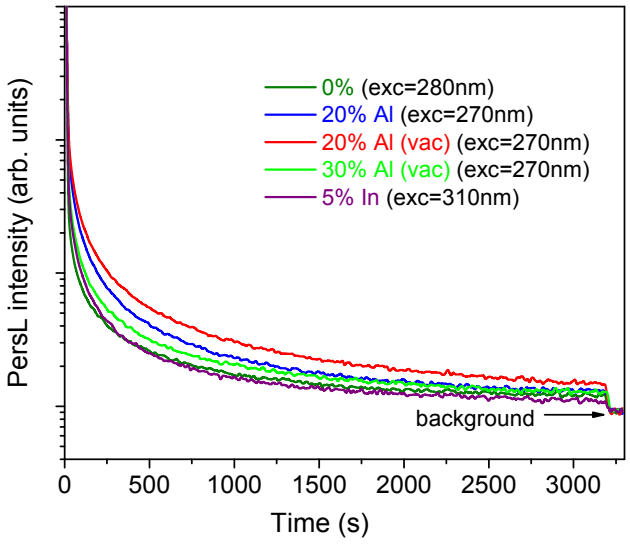

Fig. 17 Room-temperature afterglow decay kinetics of selected samples registered at 718 nm after UV (270-310 nm) exposure.

4. Conclusions

All the $Li(Ga_{1-x-y}Al_xIn_y)_5O_8$ samples synthesised by the solid-state reaction method showed a pure cubic spinel structure. Only in the materials of nominal compositions $Li(Ga_{0.9}In_{0.1})_5O_8$ and $Li(Ga_{0.8}Al_{0.14}In_{0.06})_5O_8$ with relatively higher indium content, the traces of γ-$(Ga,In)O_3$ mixed oxide were detected.

Analysis of the average *M*-O distances within the MO_6 octahedra together with the Rietveld refinement suggests unambiguously that Al^{3+} ions prefer to occupy octahedral 12*b* position (at least up to 50% of Al with respect to Ga), whereas larger In^{3+} cations mainly occupy 8*c* Ga tetrahedral site. This suggestion has also been definitely confirmed by the DFT-based electronic structure calculations, as the Al_{Ga}[*oct*] and In_{Ga}[*tetr*] substitutions protect against a noticeable increase in the total energy. The calculations also clearly reproduce the experimentally observed trends of the unit cell volume change as a function of Al or In content in the $Li(Ga_{1-x-y}Al_xIn_y)_5O_8$ alloys.

The calculations of the optical spectra of the lowest-energy $Li(Ga_{1-x-y}Al_xIn_y)_5O_8$ structures allowed to evaluate the behaviour of the optical band gap depending on the cation composition of the compounds. In particular, the replacement of 50% of Ga by Al increases the E_g value of $LiGa_5O_8$ by almost 1 eV. Indium addition, on the contrary, reduces the band gap, and this reduction is almost twice more pronounced: about 0.30 eV for 10% of In. This is well consistent with the edge of the band-to-band excitation estimated experimentally from the PLE spectra of Cr^{3+}.

The correlation between the lattice parameters (unit cell volume) and the band gap energy of the $Li(Ga_{1-x-y}Al_xIn_y)_5O_8$ samples is as follows: the smaller the unit cell volume in the $Li(Ga_{1-x}Al_x)_5O_8$ sample, the wider the band gap; conversely, the larger the unit cell volume in the $Li(Ga_{1-x}In_x)_5O_8$ sample, the narrower the band gap.

The photoluminescence spectra of $Li(Ga_{1-x-y}Al_xIn_y)_5O_8$:$Cr^{3+}$ phosphors at room temperature are featured by a narrow line emission at about 718 nm caused by the spin-forbidden $^2E \rightarrow {}^4A_2$ transition of the octahedrally-coordinated Cr^{3+} and corresponding vibronic sidebands. All the studied samples demonstrate the quantum efficiency (QE) of photoluminescence of about 50%, except the samples with 5 and 10% of Al, for which a somewhat lower QE was revealed.

The high-resolution, low-temperature photoluminescence measurements revealed a single type of Cr^{3+} centres in $LiGa_5O_8$:Cr. When Al is added, the same type of Cr^{3+} centres remains, however, the local structural disorder of the centres increases, which is evident in the broadening of the zero-phonon line (ZPL). When In is added, even greater (at the same amounts

View Article Online
DOI: 10.1039/D6DT00337K

of In and Al) broadening of ZPL is observed together with the appearance of two additional types of Cr^{3+} centres.

It was revealed that all the samples modified by Al and/or In reveal a similar TSL structure, however the position of the TSL peaks and their intensity ratios change. In particular, the position of all the TSL peaks shifts towards higher temperatures as Al content increases, and vice versa, the TSL peaks move towards lower temperatures when the host is modified by In, which is consistent with the modulation of the band gap of the host material. It was also shown that simultaneously with changing the TSL peaks position, the modification of the $LiGa_5O_8$ host by the addition of Al and/or In makes the TSL peaks broader, which means an expansion of the set of trap depths caused by local structure disorder introduced by the partial replacement of Ga atoms with Al and/or In.

The highest TSL intensity in the temperature range of 25-100 °C was found for the $Li(Ga_{0.8}Al_{0.2})_5O_8$:Cr sample annealed in vacuum, which reveals a threefold enhancement of the persistent luminescence compared to the pristine $LiGa_5O_8$:Cr sample synthesised in air.

Author contributions

Anastasiia Karabut: visialization, investigation. Halyna Zhydachevska: samples synthesis. Łukasz Wachnicki: investigation. Vasyl Hreb: writing - review&editing, investigation, visualization. Leonid Vasylechko: supervision, writing - review&editing, investigation, methodology, finding acquision, resources, visualization, writing – original draft. Yuriy Hizhnyi: writing – rewiew&editing, investigation, writing – origin draft, Tetiana Shevtsova: investigation. Andriy Luchechko: writing - review&editing, investigation. Agnieszka Pieniążek: investigation, writing - review&editing. Marek Berkowski: writing - review&editing, investigation. Yaroslav Zhydachevskyy: conceptualization, resources, funding acquisition, writing – original draft, methology. All authors have given approval to the final version of the manuscript.

Conflicts of interest

The authors declare no competing financial interest.

Data availability

The data supporting this article have been included as part of the supplementary information (SI). Supplementary information: graphical results of Rietveld refinement of the selected $LiGa_5O_8$-based spinel structures, graphical results of Rietveld refinement of chromium-doped

$LaGa_5O_8$-based materials annealed in vacuum; concentration evolution of the lattice parameters and nearest cation-oxygen distances in the $Li(Ga_{1-x}M_x)_5O_8$ series; the 2×2×2 super-cell of $LiGa_5O_8$ crystal; numbers of cationic substitutions modeled in 2×2×2 super-cell of $Li(Ga_{1-x-y}Al_xIn_y)_5O_8$; DFT-optimised lattice parameters of $Li(Ga_{1-x-y}Al_xIn_y)_5O_8$ alloys; calculated low-energy parts of absorption spectra of $Li(Ga_{1-x-y}Al_xIn_y)_5O_8$ crystals; comparison of the TSL curves of the studied samples (as-synthesised and annealed in vacuum), the PLE spectra of the studied samples measured using synchrotron irradiation at room temperature (registered at 718 nm), and their deconvolution by Gaussian peaks.

Acknowledgements

The work was supported in parts by the Polish National Science Centre (project no. 2024/53/B/ST11/01108), the Ministry of Education and Science of Ukraine (project DB/GALIO no. 0125U001768), the National Research Foundation of Ukraine (grant no. 2025.07/0218), and the European Research Executive Agency (HORIZON-MSCA-2023-SE-01 Project no. 101182995). The authors gratefully acknowledge Polish high-performance computing infrastructure PLGrid (HPC Centre: ACK Cyfronet AGH) for providing computer facilities and support within the computational grant no. PLG/2024/017683. This work also received funding from the European Union through Project 101120397 – APPROACH. The assistance of Dr. Oksana Chukova in taking measurements using synchrotron radiation is warmly acknowledged.

References

1. P. Zhang, X. Chen, Y. Bai, X. Zhao, X. Fu, L.Wu, Y. Wang, T. Sun, Y. Kong, Y. Zhang, J. Xu, Quasi-Continuous Defects Levels in Broadband Gap: A new strategy for high-temperature long persistent luminescence materials, *Optical Materials,* 2024, **12**, 2301406, DOI: https://advanced.onlinelibrary.wiley.com/doi/full/10.1002/adom.202301406
2. X. Lu, Y. Wang, J. Yang, P. D. Townsend, D. Hreniak, $LiGa_5O_8$:Fe^{3+}: A novel and super long mear-infrared persistent material, *Ceramics International A* 2024, **19**, 35359-35367, DOI: https://www.sciencedirect.com/science/article/abs/pii/S0272884224027822
3. S. Wu, P. Xiong, K. Qin, Y. Xiao, B. Xiao, K. Chen, D. Jiang, Y. Wang, Ratiometric mechanoluminescence in single Pr^{3+}-actived $LiGa_5O_8$, *Luminescence,* 2023, **38** (8), 1465-1476, DOI: https://analyticalsciencejournals.onlinelibrary.wiley.com/doi/10.1002/bio.4528
4. S. Lu, J. Wang, Q. Zhu, Differential substitution of Ga^{3+} by Mn^{2+} and Cr^{3+} in $LiGa_5O_8$ to prepare multi-mode fluorescent materials as array elements for anti-counterfeiting, *Journal of Alloys and Compounds,* 2024, **1003**, 175567, DOI: https://www.sciencedirect.com/science/article/abs/pii/S0925838824021546?via%3Dihub
5. N. I. Singh, L. L. Singh, A. N. Singh, L. R. Singh, S. B. Singh, Thermoluminescence analysis of NIR persistent phosphors (LGO:Cr) synthesized using sol-gel and solid-state methods, *Journal of Electronic Materials,* 2024, **53**, 4848-4856. DOI: https://link.springer.com/article/10.1007/s11664-024-11208-4
6. X. Yang, X. Zhang, Y. Hu, Y. Jia, Y. Wang, S. Yun, D. Gao, A phenomenological theory about effective afterglow centers in persistent luminescence phosphors, *Journal of Alloys and Compounds,* **2025**, *1016*, 178893, DOI: https://www.sciencedirect.com/science/article/abs/pii/S0925838825004517?via%3Dihub
7. K. Dabsamut, K. Takahashi, W. R. L. Lambrecht, Native defects and their complexes in spinel $LiGa_5O_8$, *Journal of Applied Physics,* 2024, **135**, 235707, DOI: https://pubs.aip.org/aip/jap/article/135/23/235707/3298664/Native-defects-and-their-complexes-in-spinel
8. J. L. Lyons, Deep polaronic acceptors in $LiGa_5O_8$, *Journal of Applied Physics* 2024, **135**, 165705, DOI: https://pubs.aip.org/aip/jap/article/135/16/165705/3285536/Deep-polaronic-acceptors-in-LiGa5O8
9. M. Jia, X. Zhang, X. Yang, Z. Lin, D. Jia, Y. Wang, S. Yun, D. Gao, The self-activated $LiGa_5O_8$ storage phosphors: insights into its photo/thermo/mechano-stimulated NIR luminescence, *Journal of Materials Chemistry C,* 2025, **9**, 4616-4625, DOI: https://pubs.rsc.org/en/content/articlelanding/2025/tc/d4tc04818k
10. Ya. Zhydachevskyy, Y. Hizhnyi, S. G. Nedilko, I. Kudryavtseva, V. Pankratov, V. Stasiv, L. Vasylechko, D. Sugar, A. Lushchik, M. Berkowski, A. Suchocki, N. Klyui, Band gap engineering and trap depths of intrinsic point defects in RAlO3 (R=Y, La, Gd, Yb, Lu) perovskites, *J. Phys. Chem. C,* 2021, **125**, 26698-26710, DOI: https://pubs.acs.org/doi/10.1021/acs.jpcc.1c06573
11. V. Stasiv, Ya. Zhydachevskyy, V. Stadnik, V. Hreb, V. Mykhaylyk, L. Vasylechko, A. Luchechko, T. Wojciechowski, P. Sybilski, A. Suchocki, Chemical tuning of photo- and persistent luminescence of Cr^{3+}-actived β-Ga_2O_3 by alloying with Al_2O_3 and In_2O_3, *J. Alloys Compd,* 2024, **982**, 173827, DOI: https://www.sciencedirect.com/science/article/abs/pii/S0925838824004146
12. C.-Y. Chang, N. Majewska, K.-C. Chen, W.-T. Huang, T. Lesniewski, G. Leniec, S. Kaczmarek, W.-K. Pang, V. Peterson, D.-H. Cherng, K.-M. Lu, S. Mahlik, R.-S. Liu, Ultrahigh quantum efficiency near-infread-Ⅱ emission achieved by Cr^{3+} clusters to Ni^{2+} energy transfer, *Chemistry of Materials,* 2022, **34**, 10190–10199, DOI: https://pubs.acs.org/doi/10.1021/acs.chemmater.4c00438
13. J.-L. Hsu, R.-J. Chung, N. Majewska, D. Kreft, H.-S. Sheu, J.-F. Lee, S. Mahlik, M. H. Fang, Probing local structural changes by sharp luminescent infrared nanophosphors for

application in light-emitting diodes, *Chem. Mater*, 2022, **34**, 11093-11100, DOI: https://pubs.acs.org/doi/10.1021/acs.chemmater.2c03224

14. M. Kaminski, Y.-T. Tsai, Y.-L. Kuo, A. Mnnoz, U.R. Mendoza, M.-H. Fang, S. Mahlik, Exploring near-infrared luminescence of Ni^{2+} in $Li(Ga,Al)_5O_8$:spinels via mechanical and chemical pressure, *Chem. Mater*, 2026, ***38*** (24) DOI: https://doi.org/10.1021/acs.chemmater.5c02959.

15. O. M. Sousa, Study of the structural, electronic, and optical properties of the host matrices of $LiAl_5O_8$ and $LiGa_5O_8$ via DFT, *Computational and Theoretical Chemistry*, 2018, **1123**, 96–101, DOI: https://www.sciencedirect.com/science/article/pii/S2210271X17304929

16. O. M. Sousa, I. P. Carvalho, Theoretical study of the structural, energetic, electronic and magnetic properties of the host matrix $LiGa_5O_8$ doped with Cr^{3+}, *Journal of Solid State Chemistry,* 2020, **289**, 121472, DOI: https://www.sciencedirect.com/science/article/abs/pii/S0022459620303029?via%3Dihub

17. W. Lambrecht, Spinel $LiGa_5O_8$ prospects as ultra-wideband-gap semiconductor: band structure, optical properties, and doping, *J. Vac. Sci. Technol. A,* 2024, **42**, 022705, DOI: https://pubs.aip.org/avs/jva/article/42/2/022705/3263554/Spinel-LiGa5O8-prospects-as-ultra-wideband-gap

18. L. Akselrud, Y. Grin, WinCSD: software package for crystallographic calculations (Version 4), *J. Appl. Crystallogr,* 2014, **47**, 803–805, DOI: https://journals.iucr.org/paper?S1600576714001058

19. Ya. Zhydachevskyy, I. Syvorotka, V. Tsiumra, M. Baran, L. Lipińska, A. Wierzbicka, A. Suchocki, Quantum efficiency of the down-conversion process in Bi^{3+}-Yb^{3+} and Ce^{3+}-Yb^{3+} co-doped garnets, *Solar Energy Materials and Solar Cells*, 2018, **185**, 240–251, DOI: https://www.sciencedirect.com/science/article/abs/pii/S0927024818302642?via%3Dihub

20. Y. Smortsova, O. Chukova, M. Kirm, V. Nagirnyi, V. Pankratov, A. Kataev, A. Kotlov, The P66 time-resolved VUV spectroscopy beamline at PETRA III storage ring of DESY, *Journal of Synchrotron Radiation,* 2025, **32**, 1539–1548, DOI: 10.1107/S1600577525007568

21. BIOVIA Materials Studio, An Integrated, Multi-Scale Modeling Environment, https://www.3ds.com/productsservices/biovia/products/molecular-modeling-simulation/biovia-materials-studio, (accessed on 22 January 2025).

22. J. P. Perdew, K. Burke, M. Ernzerhof, Generalized gradient approximation made simple, *Phys. Rev. Lett,* 1996, **77** (18), 3865-2868, DOI: https://journals.aps.org/prl/abstract/10.1103/PhysRevLett.77.3865

23. B.G. Pfrommer, M. Côté, S. G. Louie, M. L. Cohen, Relaxation of crystals with the quasi-Newton method, *J. Comput. Phys,* 1997, ***131***, 233–240, DOI: https://www.sciencedirect.com/science/article/pii/S0021999196956120?via%3Dihub

24. G. Kresse, D. Joubert, From ultrasoft pseudopotentials to the projector augmented-wave method, *Phys. Rev. B,* 1999, ***59***, 1758-1775, DOI: https://journals.aps.org/prb/abstract/10.1103/PhysRevB.59.1758

25. L. Vasylechko, V. Hreb, Ya. Zhydachevskyy, Y. Hizhnyi, A. Smaliuk, V. Stasiv, V. Stadnik, Y. Hirskyi, H. Zhydachevska, V. Mykhaylyk, A. Suchocki, Tuning of crystal structure and electronic band gap of the monoclinic Ga_2O_3 by simultaneous alloying with Al_2O_3 and In_2O_3, *Scientific Reports*, 2025, **15** (1), 37128, DOI: https://www.nature.com/articles/s41598-025-21074-7

26. A. Tomas, P. Laruelle, J. L. Dormann, M. Noguès, Affinement de la structure des formes ordonnée et desordonnée de l'octaoxopentaferrate de lithium, $LiFe_5O_8$, *Acta Crystallogr. C,* 1983, **39**, 1615-1617, DOI: https://journals.iucr.org/paper?a22819

27. R. D. Shannon, Revised effective ionic radii and systematic studies of interatomic distances in halides and chalcogenides, *Acta Crystallogr. A,* 1976, **32**, 751–767, DOI: https://journals.iucr.org/paper?S0567739476001551

28. J. Joubert, M. Brunel, A. Waintal, A. Durif, Etude cristallographique du gallate de lithium et de sa solution solide avec l`aluminate. *Comptes Rendus Hebdomadaires des Seances de l'Academie des Sciences (1884 - 1965),* 1963, **256**, 5324-5326, DOI: https://next-gen.materialsproject.org/materials/mp-28146

29. S. Sasaki, C.T. Prewitt, R. C. Liebermann, The crystal structure of $CaGeO_3$ perovskite and the crystal chemistry of the $GbFeO_3$-type pervoskites, *Am. Mineral*, 1983, 68, 1189, DOI: https://msaweb.org/AmMin/AM68/AM68_1189.pdf

30. K. Zhang, V. G. T. Vangipuram, H.- L. Huang, J. Hwang, H. Zhao, Discovery of a robust p-type ultrawide bandgap oxide semiconductor: $LiGa_5O_8$, *Adv. Electron. Mater*, 2025, **11**, 2300550, DOI: https://advanced.onlinelibrary.wiley.com/doi/10.1002/aelm.202300550?utm_medium=article&utm_source=researchgate.net

31. P. Gluchowski, M. Chaika, Crystal-field strength variations and energy transfer of Cr^{3+} - doped GGG transparent nanoceramics, *The Journal of Physical Chemistry C,* 2024, **128**, 9641-9651, DOI: https://pubs.acs.org/doi/10.1021/acs.jpcc.4c01658

32. K.C. Chen, M. H. Fang, W. T. Huang, M. Kamiński, N. Majewska, T. Leśniewski, S. Mahlik, G. Leniec, S. M. Kaczmarek, C. W. Yang, K. M. Lu, H. S. Sheu, R. S. Liu, chemical and mechanical pressure-induced photoluminescence tuning via structural evolution and hydrostatic pressure, *Chemistry of Materials*, 2021, **33**, 3832–3840, DOI: https://www.ch.ntu.edu.tw/~rsliu/publications/2021/12.pdf

33. V. Mykhaylyk, H. Kraus, Ya. Zhydachevskyy, V. Tsiurma, A. Luchenchko, A. Wagner, A. Suchocki, Multimodal non-contact luminescence thermometry with Cr-doped oxidas, *Sensors*, 2020, **20** (18), 5259, DOI: https://www.mdpi.com/1424-8220/20/18/5259

34. Ya. Zhydachevskyy, V. Mykhaylyk, V. Stasiv, L.-I. Bulyk, V. Hreb, I. Lutsyuk, A. Luchechko, S. Hayama, L. Vasylechko, A. Suchocki, Chemical tuning, pressure, temperature behavior of Mn^{4+} photoluminescence in Ga_2O_3- Al_2O_3 alloys, *Inorganic Chemistry*, 2022, **65**, 18135-18146, DOI: https://pubs.acs.org/doi/10.1021/acs.inorgchem.2c02807

35. M. Chaika, Temperature-depend spectroscopy of Cr^{3+}:YGG nanophosphors with multisite emission, *Materials Research Bulletin*, 2025, **195**, 113841, DOI: https://www.sciencedirect.com/science/article/abs/pii/S0025540825005483?via%3Dihub

36. Z. Yi, P. Liu, X. Liu, Y. Xu, Prolonged red persistent luminescence in Bi^{3+} single-doped $LiGa_5O_8$: regulating traps by site selective occupation. *Inorganic Chemistry*, 2023, **62**, 19542-19551, DOI: https://pubs.acs.org/doi/10.1021/acs.inorgchem.3c02720

TOC Graphic

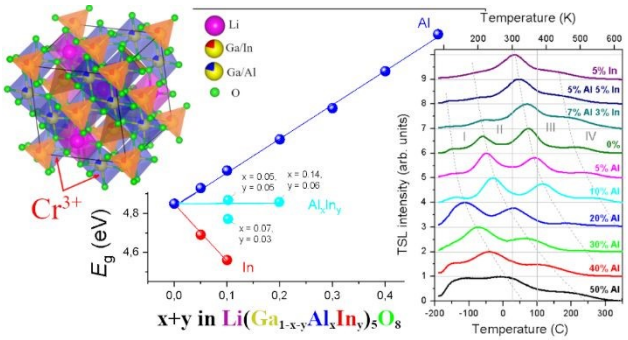

View Article Online
DOI: 10.1039/D6DT00337K

Data availability

The data supporting this article have been included as part of the supplementary information (SI). Supplementary information: graphical results of Rietveld refinement of the selected $LiGa_5O_8$-based spinel structures, graphical results of Rietveld refinement of chromium-doped $LaGa_5O_8$-based materials annealed in vacuum; concentration evolution of the lattice parameters and nearest cation-oxygen distances in the $Li(Ga_{1-x}M_x)_5O_8$ series; the 2×2×2 super-cell of $LiGa_5O_8$ crystal; numbers of cationic substitutions modeled in 2×2×2 super-cell of $Li(Ga_{1-x-y}Al_xIn_y)_5O_8$; DFT-optimised lattice parameters of $Li(Ga_{1-x-y}Al_xIn_y)_5O_8$ alloys; calculated low-energy parts of absorption spectra of $Li(Ga_{1-x-y}Al_xIn_y)_5O_8$ crystals; comparison of the TSL curves of the studied samples (as-synthesised and annealed in vacuum), the PLE spectra of the studied samples measured using synchrotron irradiation at room temperature (registered at 718 nm), and their deconvolution by Gaussian peaks.